UNIVERSITY OF CALIFORNIA,
IRVINE

Impact of Extracellular Matrix Structure and Integrin Expression on Human Fibroblast Phenotype

DISSERTATION

submitted in partial satisfaction of the requirements
for the degree of

DOCTOR OF PHILOSOPHY

in Biomedical Engineering

by

Nicholas Joseph Merna

Dissertation Committee:
Professor Steven C. George, Chair
Associate Professor Bernard H. Choi
Assistant Professor Anna Grosberg

2014

DEDICATION

To

my parents and friends

in recognition of their support

"Come potreste descrivere a parole questo cuore,
senza riempire un libro intero?"
(How could you describe this heart in words,
without filling a whole book?)

Note written by Leonardo da Vinci beside an anatomical
drawing of the heart, 1513.

TABLE OF CONTENTS

LIST OF FIGURES

LIST OF TABLES

ACKNOWLEDGMENTS

I would like to express my deepest gratitude to my committee chair, Professor Steven C. George, whose enthusiasm and encouragement were key motivations throughout my PhD. Without his guidance this dissertation would not have been possible.

I would like to thank my committee members, Professor Bernard H. Choi and Professor Anna Grosberg, for their time and support.

I thank Mary Ann Liebert, Inc. for permission to include Chapter One of my dissertation. Chapter One is a copy of an article published in Tissue Engineering © 2013 copyright Mary Ann Liebert, Inc.; Tissue Engineering is available online at: http://online.liebertpub.com. This work has been supported in part by a grant from the National Institutes of Health (R01 HL067954 to SCG), as well as the Laser Microbeam and Medical Program (LAMMP) at the Beckman Laser Institute. The LAMMP facility is supported by the National Institutes of Health (NIH P41 EB015890). We would also like to recognize the assistance and expertise of Dr. Tatiana Krasieva at the Beckman Laser Institute for MPM imaging, and Mr. Earl Steward for assistance in procuring the porcine hearts.

CURRICULUM VITAE

Nicholas Merna

2009	B.S. in Bioengineering, University of California, Los Angeles
2012	M.S. in Biomedical Engineering, University of California, Irvine
2011-13	Teaching Assistant, Graduate School of Biomedical Engineering, University of California, Irvine
2014	Ph.D. in Biomedical Engineering, University of California, Irvine

FIELD OF STUDY

Tissue Engineering and Regenerative Medicine

PUBLICATIONS

"Optical imaging predicts mechanical properties during decellularization of cardiac tissue." Merna, N., C.R. Robertson, A. La, and S.C. George. Tissue Engineering. Part C, 19(10): 10.1089/ten.TEC.2012.0720, 2013.

ABSTRACT OF THE DISSERTATION

Impact of Extracellular Matrix Structure and Integrin Expression on Human Fibroblast Phenotype

By

Nicholas Joseph Merna

Doctor of Philosophy in Biomedical Engineering

University of California, Irvine, 2014

Professor Steven C. George, Chair

Extracellular matrix (ECM) derived from whole organ decellularization offers a promising biological scaffold for tissue engineering applications. The native 3D structure and biochemical composition of these matrices can potentially support tissue-specific recellularization strategies. However, decellularization protocols use reagents that can disrupt the ECM resulting in a range of mechanical properties and protein composition. By identifying structural and biochemical features of the ECM that impact cell behavior, we can tailor decellularization protocols to retain those features. Recellularization of decellularized matrices is an intriguing strategy to engineer lung and cardiac tissue that will likely include the fibroblast. However, excessive collagen deposition by fibroblasts could interfere with normal structure and function of the surrounding tissue. Furthermore, integrin expression can influence the expression of intracellular structural proteins such as alpha smooth muscle actin (α-SMA), and extracellular structural proteins such as collagen. However, previous work has not determined the effect of decellularized ECM on fibroblast function and integrin signaling.

In this work, we used multiphoton microscopy (MPM), combined with image correlation spectroscopy (ICS), to characterize structural and mechanical properties of the decellularized cardiac matrix in a non-invasive and non-destructive fashion. ICS amplitude of second harmonic generation (SHG) collagen images (collagen content) and ICS ratio of two-photon fluorescence (TPF) elastin images (elastin alignment) strongly correlated with compressive modulus. We then seeded cardiac and lung fibroblasts on cardiac ECM, lung ECM and their components to determine the effect of substrate composition, tissue specificity and integrin expression on fibroblast phenotype. α-SMA expression increased for stiffer substrates, and lung fibroblasts expressed significantly higher levels of α-SMA than cardiac fibroblasts. Higher expression of β_3 integrins in cardiac fibroblasts, combined with increased α-SMA expression resulting from functional blocking of β_3 integrins, demonstrates that β_3 plays an important role in regulating cardiac fibroblast phenotype. Our findings indicate that ECM stiffness strongly correlates with collagen and elastin alignment in the ECM following decellularization, which can potentially impact fibroblast collagen and α-SMA expression during recellularization. Furthermore, differential expression of β_3 integrins in organ-specific fibroblasts impacts α-SMA expression suggesting that both stromal cell source and ECM structure can impact the remodeling response during recellularization.

INTRODUCTION

End-stage organ failure results in morbidity and mortality for tens of thousands of patients each year (1, 2). Approximately 425,000 patients with coronary heart disease die annually (2), 120,000 die as a result of chronic lung disease (3), and 112,000 die from end-stage kidney failure (4). The definitive treatment is allogeneic transplantation, but there is a severe shortage of donor organs, and those who are fortunate enough to receive an organ transplant are burdened with a lifelong regime of immunosuppressant therapy and risk chronic rejection (5). A successful whole organ replacement strategy that does not rely on human donor organs would represent a paradigm shift in the treatment of patients with end-stage organ failure. A promising solution is engineered tissues, which have made great progress in recent years (6, 7).

The traditional approach to engineering tissues, which has been in use for over twenty years, is to culture autologous cells on artificial scaffolds in order to generate simple tissues (**FIG I.1**) (8, 9). Cells are taken from an autologous donor, cultured as a monolayer *in vitro* and then expanded to generate the large number of cells needed to grow tissues. These cells are then seeded onto artificial scaffolds that attempt to mimic specific features of the cells' native environment**.** After weeks of culture, these tissue constructs can be implanted in animal models for additional testing.

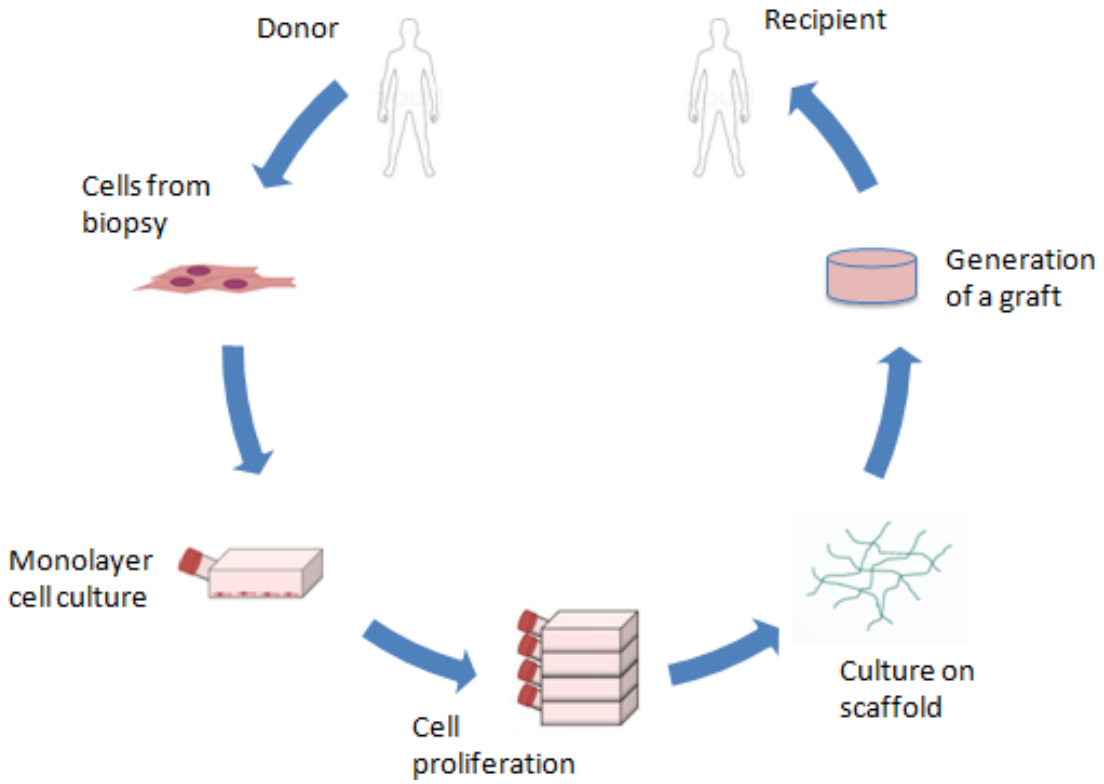

Figure I.1: Illustration of the traditional tissue engineering paradigm (10, 11).

However, the success of traditional tissue engineering approaches has been limited to simple organs, such as the skin or bladder (12, 13). There has been significantly less progress engineering complex organs like the heart or lung, for several reasons (14, 15). These organs have a more complex architecture and composition, which can be difficult to mimic with artificial scaffolds (16). Also, these organs are required to perform multiple functions in vivo. One way to recapitulate the complexity of these tissues is to use the organs' natural support structure or scaffolding -- its extracellular matrix (ECM). ECM provides tissue-specific physical and chemical cues that have been shown to promote cell functionality and viability, with minimal immune response (17, 18). There have been

efforts to create synthetic ECM analogues that mimic the native ECM; however these products have been limited in their scope to patches and skin grafts (19, 20).

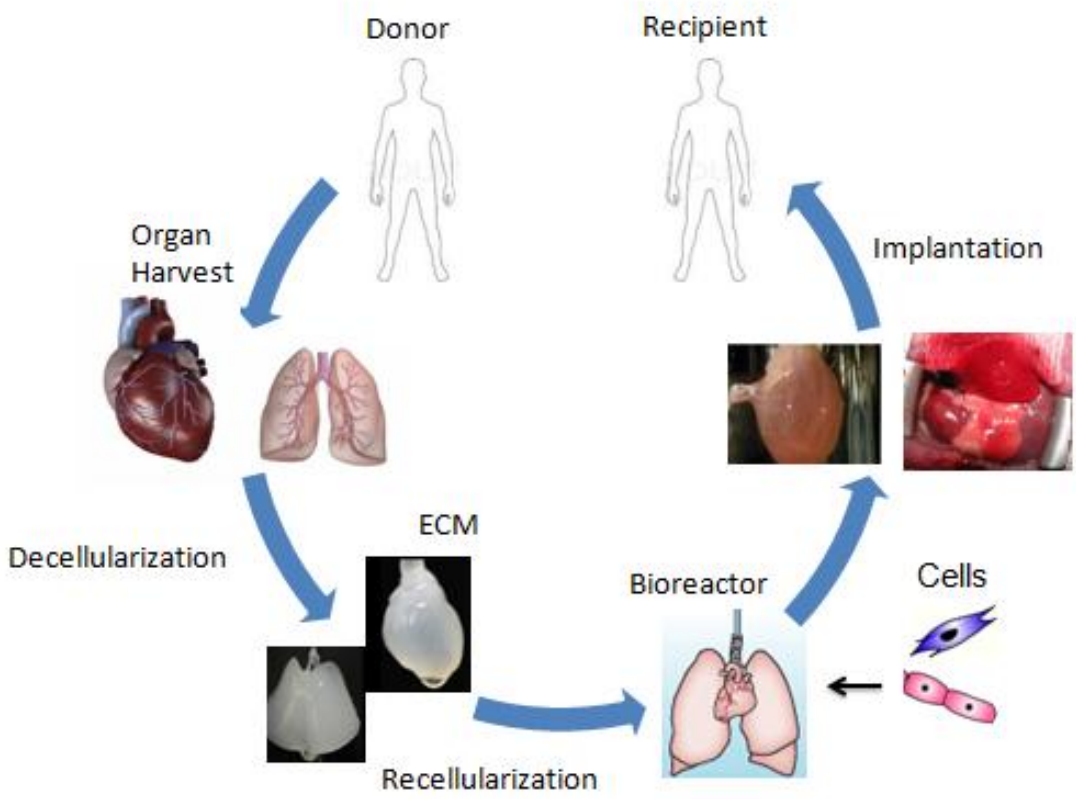

Figure I.2: Illustration of an emerging tissue engineering paradigm. Extracellular matrix is derived from whole organ decellularization and then recellularized to create whole organ constructs (21-23).

This strategy of decellularizing whole organs and recellularizing the ECM really took front stage in 2008 when Doris Taylor at the University of Minnesota recellularized murine ECM to create contractile heart tissue (21). This paradigm starts with an organ taken from a human source (in the case that the organ is not viable for transplant) or a more readily

available animal source that has an organ size and function that is similar to humans (e.g., bovine). Cells are then removed from the tissue by the process of decellularization, leaving the ECM (**FIG I.2**). Recellularization of this ECM with human cells from the potential recipient could then potentially restore function, and avoid immune rejection. This strategy has been explored by numerous groups with some success in the ability to restore at least partial function in vivo and in vitro for the heart, lung, liver and kidney (24-26).

The goal of whole organ decellularization is removal of cellular material, without impacting composition, biological activity or mechanical integrity of the ECM. Removal of cellular material is necessary to minimize an adverse immune response by recipients of the ECM. This leaves ECM proteins, which are highly conserved across species and are well tolerated in xenogeneic transplants (27, 28). The process of decellularization requires perfusion of chemical and enzymatic reagents, as well as physical methods such as freezing or agitation. However, a major limitation of decellularization is that these reagents damage the ECM which results in a loss of structure, protein content and mechanical integrity (29, 30).

Figure I.3: ECM derived from heart, lung, liver and kidney tissues (21, 22, 31, 32).

Several groups have derived ECM using these different reagents and protocols (**FIG I.3**), resulting in scaffolds with a wide range of stiffnesses (33-35). Since substrate stiffness has been shown to play important roles in regulating the phenotype and gene expression of both functional and support cells (36, 37), it will be beneficial to determine how decellularization impacts ECM stiffness. Despite this variation in ECM properties and its potential impact on cell response, there have been few studies that compare the impact of different decellularization protocols on the ECM. In addition, a comparative study on the impact of decellularization on the ECM structure has not yet been presented. By improving our understanding of the relationship between ECM structure and stiffness, decellularization protocols can be tailored to retain features of the ECM that enhance cell behavior.

Two structural proteins which have been shown to regulate tissue stiffness are collagen and elastin (38). By visualizing the impact of decellularization on these proteins, we may improve our understanding of the relationship between ECM structure and stiffness. Multiphoton microscopy (MPM) has been shown to be an effective tool for visualizing collagen and elastin (38, 39). Quantifying changes in collagen and elastin fiber structure using an image analysis technique, such as Image Correlation Spectroscopy (ICS), may provide insight about how ECM structure dictates tissue stiffness.

Once cells have been removed from a tissue by decellularization, there are a number of challenges associated with introducing new cells back into the ECM. Depending on the size of the tissue, recellularization can require anywhere from tens of millions to billions of

cells. Expanding this many cells is a time consuming and expensive process. Also, several types of cells are required to rebuild the parenchyma, vasculature and underlying support structures. For these reasons, the majority of work in this field has been done with small animal models. Their smaller organs require fewer cells and do not need an intact vascular network, since oxygenation is only limited by diffusion. Another challenge will be to avoid fibrosis. Fibrosis is the formation of excess connective tissue in an organ in response to inflammation or damage, similar to scarring in response to an injury. This excess connective tissue can destroy an organ's architecture and impair tissue function. In cardiac fibrosis, the excess production of collagen severely impairs the heart contractility (**FIG I.4**). This process of fibrosis has also been seen in recellularized ECM that has been implanted as skin grafts, where the resulting scar tissue inhibits host vascularization and impairs tissue function (40). Fibrosis will likely pose a challenge while recellularizing ECM derived from other organs, such as the heart and lungs. These limitations have made it clear that we are far from recapitulating complex organ function.

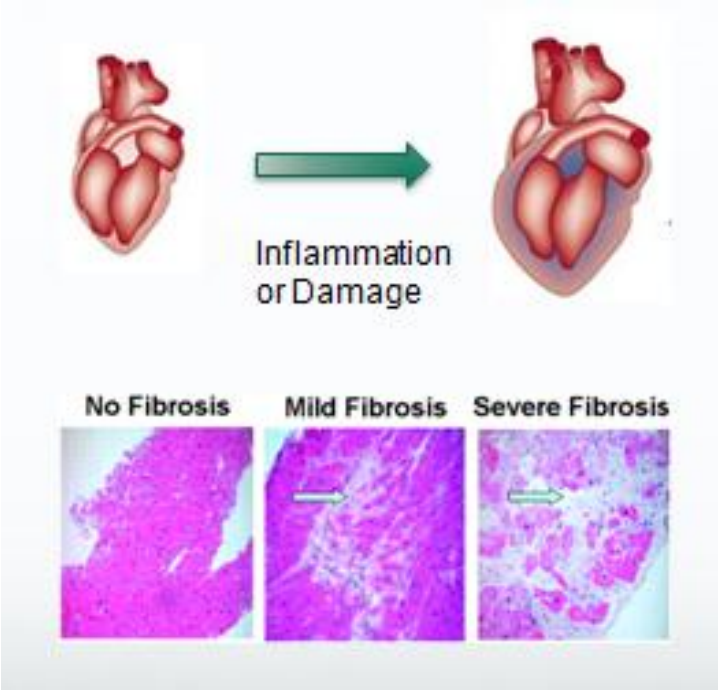

Figure I.4: Cardiac fibrosis results in excess production of collagen and loss of tissue function, shown in H&E stain (bottom) (41, 42).

However, whole organ constructs created from recellularized ECM have come a long way and different organs have had varying levels of success. For example, Doris Taylor's group had recellularized murine cardiac ECM and created contractile heart tissue. While this work was certainly the first of its kind, this heart tissue had many limitations. For example, its contractile force was only 2% of that of a fetal heart which meant that it would not be able to pump blood (21). Also, it lacked a developed vascular network and relied on diffusion to transport oxygen and nutrients. In 2010, Petersen et al. recellularized murine lung ECM that could be implanted for short times. These tissues participated in gas exchange, but lacked an alveolar barrier that could prevent leakage of blood and had poor vascular endothelial coverage (23). In 2014, Robertson et al. re-endothelialized the

vascular netwtwork of whole rat heart acellular scaffolds. This reduced thrombogenicity and enhanced ventricular contractility, but the construct lacked an intact vasculature (25). The goal of these recellularization strategies remains to achieve long term graft viability and function *in vivo*.

The goal when recellularizing ECM is to create an implantable, functional tissue by rebuilding the parenchyma, vasculature and underlying support structures. Cells are first seeded by injection or perfusion. The construct is then cultured in a perfusion bioreactor that can regulate oxygenation, culture media and biophysical stimuli. Perhaps most important is the choice of cells for recellularization. This requires functional cells that are responsible for maintaining organ function, such as cardiomyocytes in the heart, hepatocytes in the liver and epithelium in the lung. Supportive cells are also essential; endothelial cells provide a non-thrombotic barrier to confine blood flow to vascular spaces. Perhaps most important are fibroblasts, which are found throughout the body and play a prominent role in maintenance of tissue architecture through deposition of new or remodeling of existing ECM proteins. Fibroblasts have also been shown to improve parenchymal cell function in co-culture. Culture of hepatocytes with fibroblasts significantly increases liver specific functions (43), and fibroblasts aid cardiomyocytes in the propagation of electrical stimuli in the myocardium (44). Fibroblasts are also the most numerous cell type in the heart, and will therefore be essential for recellularizing the heart. For these reasons, fibroblasts will likely aid in future recellularization strategies. Fibroblasts also have site-specific gene expression and phenotype, resulting in differences in growth, metabolism and ECM protein synthesis (45). Despite the impact of fibroblasts on

matrix structure and parenchymal cell behavior, fibroblast response to decellularized ECM remains relatively unexplored.

ECM is complex and there are potentially many features that can influence fibroblast response. Substrate stiffness, cell source and substrate composition have been shown to regulate cell behavior. Different decellularization protocols have derived ECM with a wide range of mechanical properties. Interestingly, these differences in substrate stiffness have been shown to regulate the cell behavior of both functional and support cell types. Ventricular myocytes cultured on a range of substrate stiffnesses resulted in differential expression of α-actin (36). Endothelial cells and fibroblasts cultured on stiffer substrates enhanced cell spreading (37).

Fibroblasts from different areas of the body can have inherent differences in protein transcription and phenotype that may profoundly impact cell response during recellularization. An overly contractile fibroblast that produces excessive amounts of collagen can result in unwanted remodeling of the ECM. This process is most commonly seen with myofibroblasts during wound healing and fibrosis. Most importantly, organ-specific fibroblast response to ECM has not been presented. In addition to cell source, substrate composition has been shown to play an important role in regulating cell response. Each organ has a unique composition and tissue-specific ECM can best mimic a cell's extracellular environment. Previous studies have demonstrated that ECM derived from a cell's native tissue can enhance cell differentiation (seen in skeletal myoblasts) and maturation (heSC-derived cardiomyocytes), when compared to ECM from another source

(46, 47). By improving our understanding of the impact of substrate stiffness, cell source and substrate composition on fibroblast behavior we can optimize decellularization and recellularization protocols to enhance cell response to the ECM.

Integrins are membrane-bound proteins that play an important role in ECM maintenance and remodeling by transmitting signals from the ECM to regulate cell function. In the case of the fibroblast, integrins can influence the expression of intracellular and extracellular proteins, such as alpha smooth muscle actin and collagen. By determining the role integrins may play in organ-specific fibroblast response to the ECM, we may be able to identify source specific differences in cell expression that regulate fibroblast response to ECM.

A commercially available ECM scaffold that could be recellularized with selected cell populations offers a potential alternative treatment for end-stage organ failure. By identifying structural and biochemical features of the ECM that impact organ-specific fibroblast behavior and by determining what role integrins play, we may be able to improve the decellularization and recellularization process. The goal of this work is to characterize the impact of decellularization on the ECM microstructure and mechanical properties and to determine the effect of ECM structure, composition and fibroblast source on fibroblast phenotype.

CHAPTER 1: Optical Imaging Predicts Mechanical Properties During Decellularization of Cardiac Tissue

Abstract

Decellularization of xenogeneic hearts offers an acellular, naturally occurring, 3-D scaffold that may aid in the development of engineered human heart tissue. However, decellularization impacts the structural and mechanical properties of the extracellular matrix, which can strongly influence cell response during recellularization. We hypothesized that multiphoton microscopy (MPM), combined with image correlation spectroscopy (ICS), could be used to characterize structural and mechanical properties of the decellularized cardiac matrix in a non-invasive and non-destructive fashion. Whole porcine hearts were decellularized for 7 days by four different solutions of Trypsin and/or Triton. Compressive modulus of the cardiac extracellular matrix decreased to <20% of that of the native tissue in three of the four conditions (range 2-8 kPa); the modulus increased by ~ 150% (range 125-150 kPa) in tissues treated with Triton only. Collagen and elastin content decreased steadily over time for all four decellularization conditions. ICS amplitude of second harmonic generation (SHG, A_{SHG}) collagen images increased in three of the four decellularization conditions characterized by a decrease in fiber density; ICS amplitude was approximately constant in tissue treated with Triton only. The ICS ratio (R_{SHG}, skew) of collagen images increased significantly in the two conditions characterized by loss of collagen crimping or undulations. ICS ratio of two-photon fluorescence (TPF, R_{TPF}) elastin images decreased in three of the four conditions, but increased significantly in Triton only

treated tissue characterized by retention of densely packed elastin fibers. There were strong linear relationships between both the log of A_{SHG} (R^2 = 0.86) and R_{TPF} (R^2 = 0.92) with the compressive modulus. Using these variables, a linear fit predicts the compressive modulus: E = 73.9*Log(A_{SHG}) + 70.1*R_{TPF} – 131 (R^2=0.94). This suggests that collagen content and elastin alignment determine mechanical properties of the extracellular matrix. We conclude that MPM and ICS analysis is a non-invasive, non-destructive method to predict the mechanical properties of the decellularized cardiac extracellular matrix.

Introduction

Decellularization of xenogeneic hearts offers an instructive extracellular matrix (ECM) that may facilitate the development of engineered human heart tissue. Porcine cardiac extracellular matrix (C-ECM) has been shown to promote functionality and viability of avian cardiomyocytes and murine mesenchymal stem cells, without eliciting an immune response upon implantation (48, 49). Additionally, C-ECM potentially retains the physical and chemical cues to aid cells in proliferation and spatial re-organization (21, 48, 49).

The decellularization process affects the ECM composition, structure, and mechanical properties (50), which have been shown to affect cell response upon re-seeding. For example, the substrate stiffness significantly impacts immature ventricular myocyte maturation and differentiation (51). In addition, cells cultured on collagen gels with stiffness similar to native myocardium demonstrate improved function and phenotype. They are more likely to beat, beat with greater frequency, develop aligned sarcomeres and

generate greater contractile force (51-53). Furthermore, previous work has generally cultured cardiomyocytes on collagen coated gels that have stiffnesses similar to native myocardium, but lack structural features present in native tissue such as collagen crimping or undulations (51, 52). Network microstructure can affect the mechanical properties of the extracellular matrix (54, 55). Thus, retaining both the mechanical properties and structural features of native myocardium will likely improve the performance of seeded cardiomyocytes during recellularization.

Imaging the collagen and elastin fibers of C-ECM may improve our understanding of the relationship between mechanical properties and cell response. Multiphoton microscopy (MPM) and image correlation spectroscopy (ICS) are an effective combination to non-invasively and non-destructively assess bulk mechanical properties of collagen hydrogels (39, 56, 57), and may be useful for *in vivo* applications, including the assessment of elastin (38). However, previous work has not considered additional structural features, such as collagen crimping, which is present in the natural ECM. It is not well understood how these structural features affect mechanical properties. The goal of the current work is to quantitatively and non-invasively characterize the impact of decellularization on the C-ECM microstructure and mechanical properties using MPM and ICS.

Materials and Methods

Preparation of C-ECM

Whole porcine hearts were obtained immediately after euthanasia of 40-55 kg, adult female Yorkshire pigs. Excess fat and connective tissue were removed, and the coronaries were perfused with phosphate buffered saline to remove coagulated blood. Each heart was frozen at -80 ^{o}C for at least 24 hours to aid in cell lysis (48). These hearts were then thawed at room temperature and decellularized over a seven day period by coronary perfusion with four different solutions of either Trypsin/EDTA/NaN_3 and/or Triton/EDTA/NaN_3 (Table 1.1) as previously described (48). All Trypsin conditions were at a concentration of 0.02% and all Triton conditions were at a concentration of 3%. All solutions contained 0.05% EDTA and 0.05% $NaNa_3$. Different combinations of Trypsin and Triton were used as their mechanism of action should differentially impact the extracellular matrix (48, 58). Full thickness left ventricular tissue samples (1x1cm) were collected every 24 hours for imaging of MPM of fiber ultrastructure, mechanical testing for compressive modulus and protein analysis of collagen, elastin and DNA content.

Table 1.1: Decellularization Conditions

Decell 3/4	0.02% Trypsin/ 0.05% EDTA/ 0.05% NaN_3 for 3 days and 3% Triton X-100/ 0.05% EDTA/ 0.05% NaN_3 for 4 days
Decell 1/6	0.02% Trypsin/ 0.05% EDTA/ 0.05% NaN_3 for 1 days and 3% Triton X-100/ 0.05% EDTA/ 0.05% NaN_3 for 6 days
Tryp Only	0.02% Trypsin/ 0.05% EDTA/ 0.05% NaN_3 for 7 days
Trit Only	3% Triton X-100/ 0.05% EDTA/ 0.05% NaN_3 for 7 days

Multiphoton Microscopy

For MPM imaging, multiphoton excited autofluorescence (elastin) and second harmonic generation (collagen) were measured (Zeiss LSM 510 Meta Microscopy System) at 5 μm intervals with depths ranging from 0 to 50 μm as previously described (56). Second harmonic generation (SHG) arises from non-linear interactions between the incident light and the non-centrosymmetric structure of fibrillar collagen, and thus uniquely reflects fibrillar collagen for *in vitro* and *in vivo* samples (59). Two-photon fluorescence (TPF) arises primarily from the autofluorescence of elastin (60). Thus, MPM enables non-invasive visualization of collagen and elastin in intact, unstained tissues. The TPF and SHG signals were collected using a 40x / 1.3 Achroplan oil-immersion objective. A circularly polarized Chameleon laser was focused on the C-ECM samples with a wavelength of 860 nm and an incident power ranging from 60-175 mW. The SHG collagen signal was obtained using a 390-465 nm bandpass filter. TPF signal was collected simultaneously in a second channel, using a 500-550 nm bandpass filter. To maximize consistency, images from different days and from different animals were taken using the same set of optical parameters, such as gain and laser intensity.

Image Correlation Spectroscopy

ICS was performed on SHG and TPF images during decellularization to quantify image morphology using indices that reflect fiber alignment and fiber density. ICS employs autocorrelation of two-dimensional and spatially resolved data (56, 61, 62) to assess fiber orientation, alignment, size, and density (56). MATLAB was first used to compute the two-dimensional spatial autocorrelation function (ACF) as previously described (56). Briefly, the ACF was calculated by first multiplying the two-dimensional spatial fast Fourier

transform (FFT) function of the image and its complex conjugate to get the power spectral density (PSD). The inverse FFT of the PSD produced the ACF. The central 32x32 pixel portion of the ACF was then cropped to remove higher spatial lag. The cropped ACF was then fit to a two-dimensional Gaussian function, where σ_M and σ_m represented the standard deviated along the major and minor axis, respectively, R_{SHG} and R_{TPF} the ratios of σ_M and σ_m for SHG and TPF images, θ the orientation of the axis with respect to the horizontal, and A_{SHG} and A_{TPF} the peak amplitudes for SHG and TPF images, respectively (Fig. 1.1). Since we could not control the orientation of our image relative to a fixed structure feature in the heart, θ was not used in this study. *A* and *R* were used as indices that reflect fiber density and alignment (62).

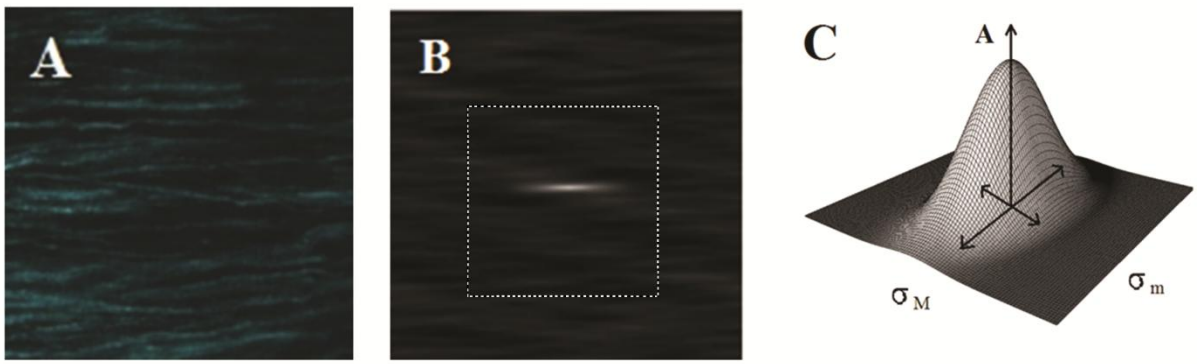

Figure 1.1: Illustration of image correlation spectroscopy**.** A) An SHG image with collagen fibers oriented horizontally, B) the autocorrelation function (ACF) of panel A, and C) the Gaussian fit of the centrally cropped ACF (dashed rectangle/square in panel B) with a wireframe representing the fit. *A* represents the peak amplitude, σ_M and σ_m represent the standard deviated along the major and minor axis.

Mechanical Testing

The compressive modulus of the tissues was measured via indentation testing (Synergie 100, MTS Systems Corporation, Eden Prairie). Sample height (~15 mm) was measured using a linear extensor. Each sample was then compressed to 20% strain with a 5 mm radius plate at a rate of 0.02 mm/s. Data was acquired with a 10N load cell at 50 Hz with 12 bit data acquisition. Modulus was calculated in the linear region of the stress-strain curve. Each sample was tested in 5 locations and the values averaged.

Protein Quantification

Total collagen, elastin and DNA content per dry weight were assessed (N=3 for each time point) using commercially available kits (collagen: hydroxyproline assay kit Cedarlane, Elastin: Fastin assay kit Biocolor, DNA: Quant-iT PicoGreen dsDNA assay Invitrogen) following the manufacturer's instructions.

Statistical Analysis

SHG and TPF image parameters, compressive modulus, DNA content, collagen content, and elastin content were analyzed as a function of time during decellularization using one-way ANOVA. Compressive modulus was compared to A_{SHG}, A_{TPF}, R_{SHG} and R_{TPF} using linear regression. In some cases a log transformation was used to determine if a power law relationship between variables was evident. Logistic regression and backward stepwise variable selection method using A and R from the both SHG and TPF was applied to find the best variables to predict compressive modulus using the Akaike information criterion (AIC) (63). Multiple linear regression was then used to determine the relationship between the

variables which had been selected by the AIC. SigmaStat was used to perform the statistical tests.

Results

Visual appearance and DNA content

All four decellularization protocols removed the red-brown coloration of the tissue by day 3. By day 7, the hearts from the four conditions were visually similar, with the exception modest differences in shape (Fig. 1.2). Hearts decellularized by Trypsin/EDTA/NaN_3 for 3 days and Triton/EDTA/NaN_3 for 4 days (Decell 3/4) or by Trypsin/EDTA/NaN_3 for 1 day and Triton/EDTA/NaN_3 for 6 days (Decell 1/6) retained their native shape. In contrast, hearts decellularized by Trit Only resembled hearts suffering from dilated cardiomyopathy with enlarged left ventricles, while hearts decellularized by Tryp Only appeared to uniformly lose shape. Quantitative analysis of DNA content of hearts decellularized by Decell 3/4 and Decell 1/6 showed a significant decrease in DNA compared to the DNA present in the non-decellularized samples (Table 1.2). This represented a 90% and 91%, respectively, decrease in the amount of double-stranded DNA present in the tissue after decellularization. Tryp Only and Trit Only resulted in incomplete decellularization with DNA removal of approximately 59% and 40%, respectively (mean ± SD of 3.39 ± 0.54 and 4.89 ± 0.37, respectively).

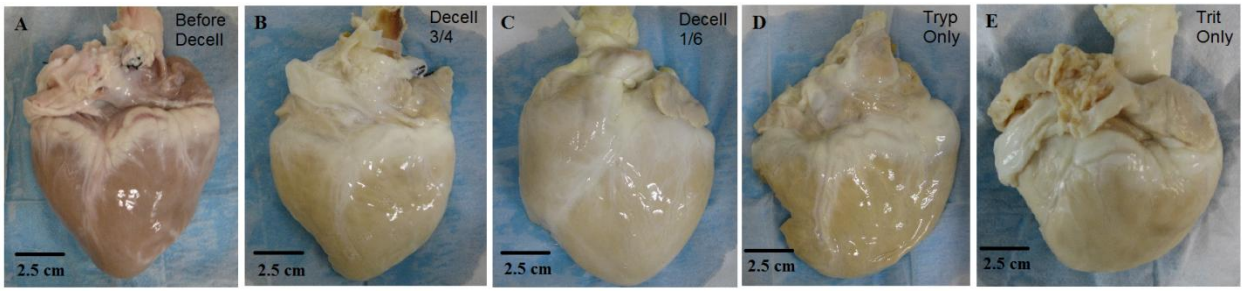

Figure 1.2*:* Representative images of intact porcine hearts decellularized by coronary perfusion are shown (A) before decellularization, (B) after 0.02% Trypsin for 3 days and 3% Triton X-100 for 4 days, (C) after 0.02% Trypsin for 1 day and 3% Triton X-100 for 6 days, (D) after 0.02% Trypsin for 7 days, and (E) after 3% Triton X-100 for 7 days.

Table 1.2: Extracellular Matrix DNA Quantification

Sample	*DNA (ng/mg dry weight)*
Native Heart	8.20 ± 0.61
C-ECM (Decell 3/4)	0.82 ± 0.18
C-ECM (Decell 1/6)	0.75 ± 0.10
C-ECM (Tryp Only)	3.39 ± 0.54
C-ECM (Trit Only)	4.89 ± 0.37

Mechanical properties, collagen and elastin content

Decellularization progressively decreased the compressive modulus of the C-ECM to < 20% of non-decellularized tissues in three of the four conditions (Fig. 1.3A). For Trit Only, the compressive modulus increased by ~ 150% by day 3, and then remained constant. In contrast, the collagen content decreased steadily over time for all of the conditions (Fig.

1.3B), although Trit Only decreased the least (~ 40% compared to ~ 80% for the other three conditions). Elastin content also decreased steadily over time for all four conditions (Fig. 1.3C). Again, Trit Only decreased the least (~30% compared to 50-70%).

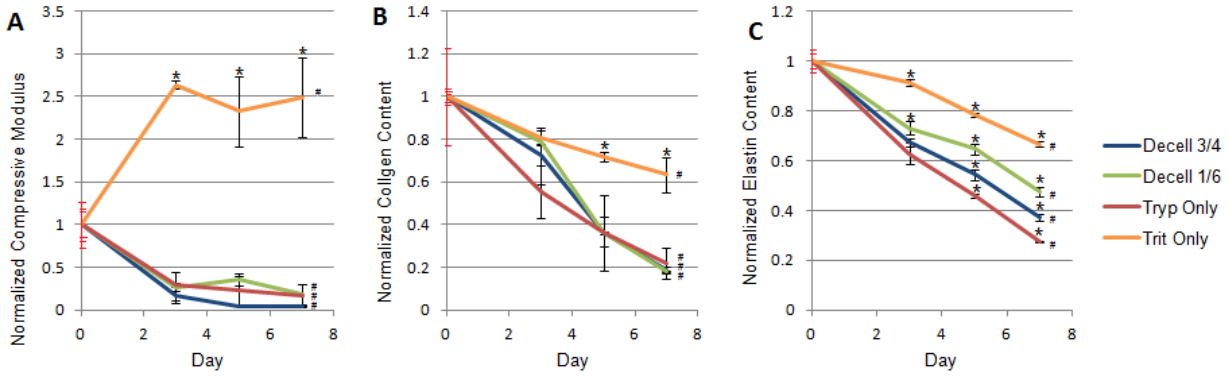

Figure 1.3: Compressive Modulus (Figure 1.3A), Collagen Content (Figure 1.3B) and Elastin Content (Figure 1.3C) measured at days 0, 3, 5 and 7 of decellularization for all 4 decellularization conditions and normalized to day 0. Baseline compressive modulus for intact samples: 61.9, 31.5, 45.0, and 31.5kPa. Baseline collagen content for intact samples: 465.6, 486.4, 503.3, and 505.3 ug/mg. Baseline elastin content for intact samples: 37.8, 37.7, 38.6, and 38.8 ug/mg. Error bars at day 0 (in red) denote standard deviation of baseline values, normalized to the average baseline value (calculated separately for each condition). Error bars for subsequent days (in black) denote standard deviation of the normalized values. Asterisks represent statistically significant differences between conditions for that day (*$p < 0.05$). Number signs represent statistical variation with time for that condition ($p < 0.05$).

Collagen microstructure

The SHG images of C-ECM at day 0 showed similar collagen fiber structure between samples, with small differences in collagen crimping. However, SHG images demonstrated significant qualitative differences between the decellularization conditions (Fig. 1.4). Decell 3/4 and Tryp Only produced C-ECM with straight and aligned collagen fibers, while Decell 1/6 and Trit Only produced C-ECM with crimped collagen fibers. These patterns began to emerge three days after initiation of the decellularization protocol.

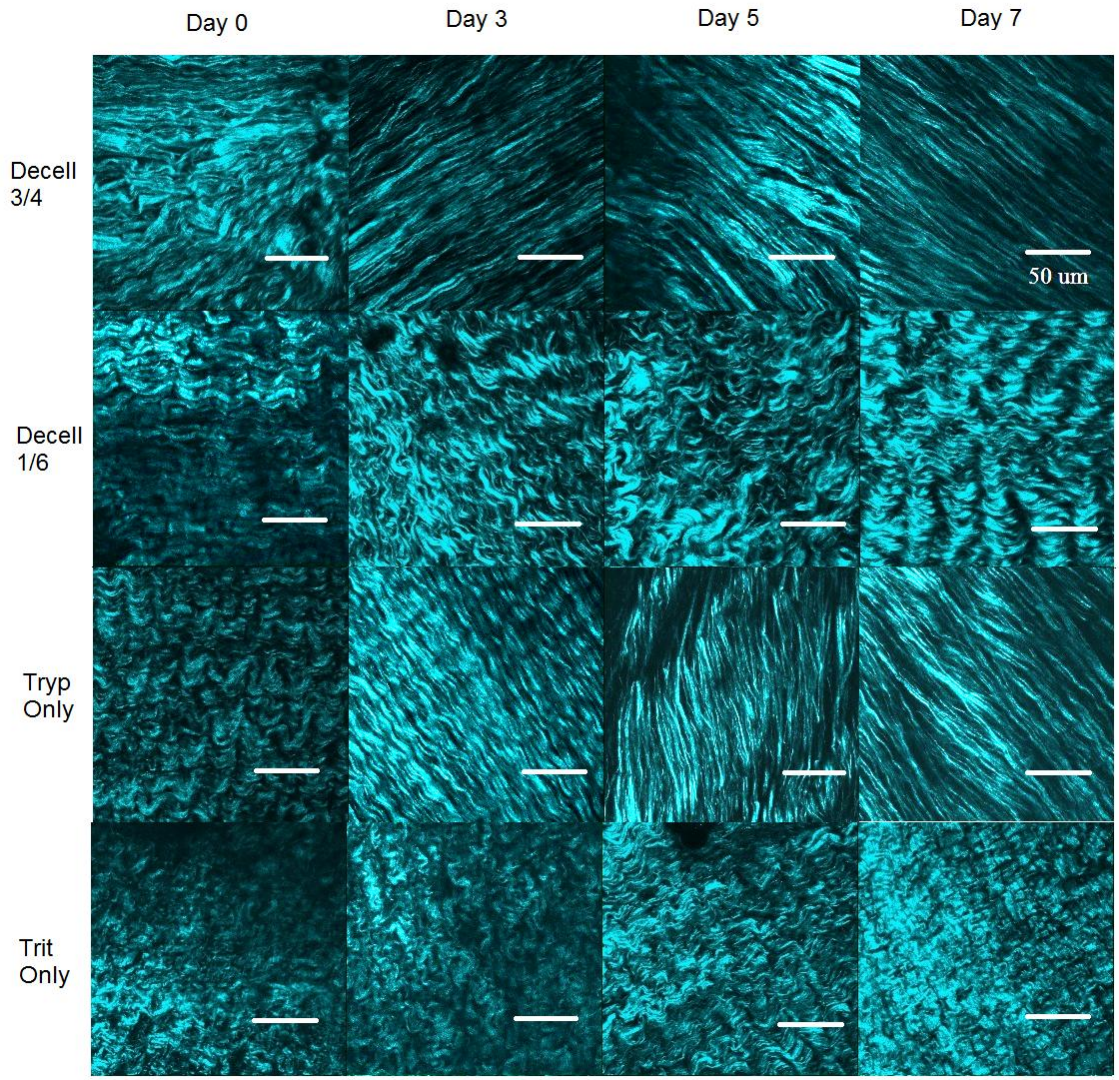

Figure 1.4. Collagen Microstructure. Representative SHG images reveal the fibrillar collagen microstructure of intact porcine hearts at days 0, 3, 5 and 7 for all 4 decellularization conditions. Images are 1024 x 1024 pixels and 230 μm x 230 μm. N=8 images per condition were used for image analysis and statistics. Scale bar 50 μm.

Elastin microstructure

The elastin microstructure can be visualized from the TPF signal (60) (Fig. 1.5). The TPF images of C-ECM at day 0 showed similar elastin fiber structure between samples, with small differences in fiber density. However, there were marked qualitative differences between the decellularization conditions. Decell 3/4, Decell 1/6 and Tryp Only significantly disrupted the fine fiber architecture present in the native tissue. In contrast, the elastin structure was largely retained in Trit Only, but the fibers appeared more densely packed.

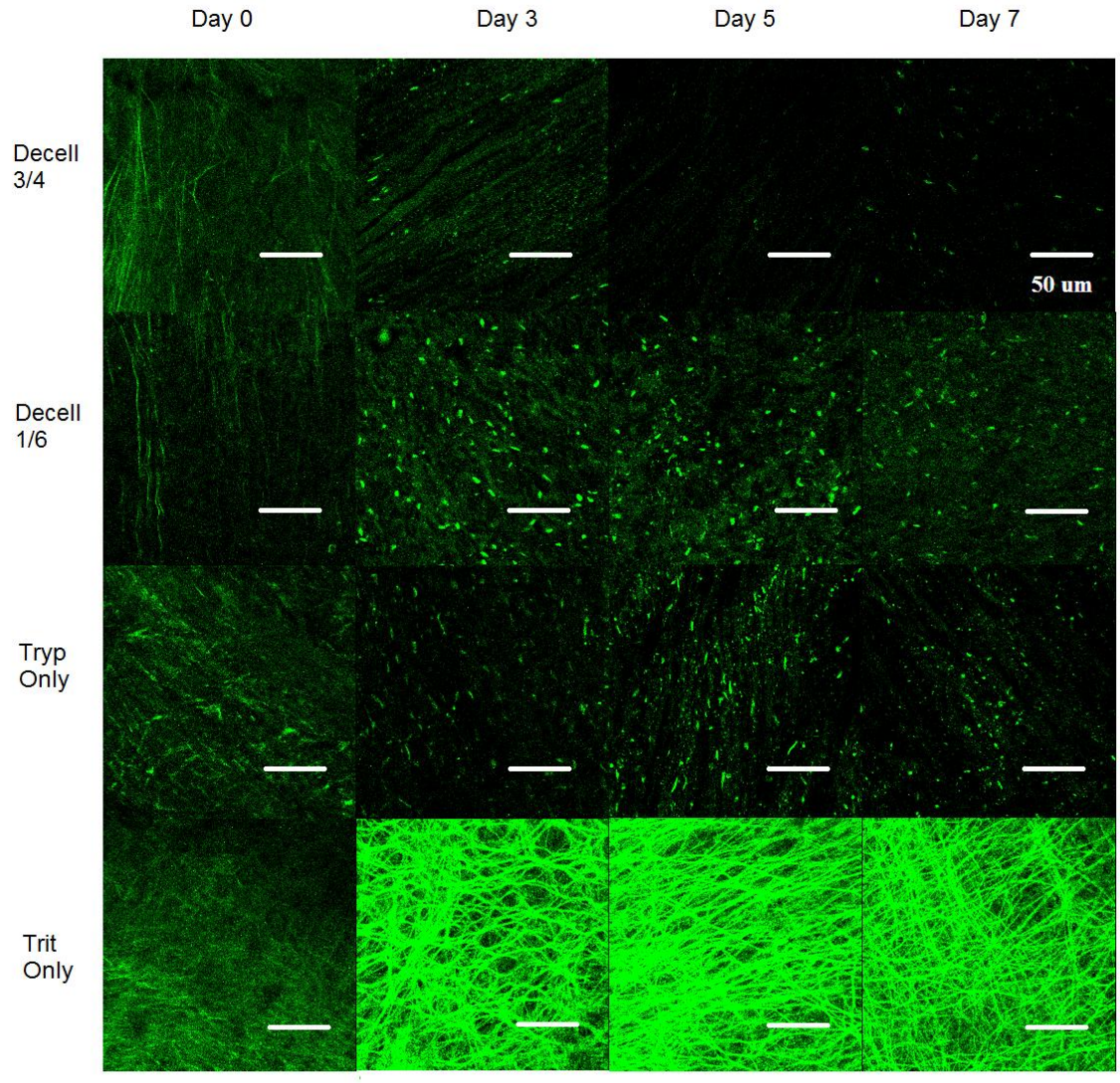

Figure 1.5. Elastin Microstructure. Representative TPF images reveal the elastin microstructure of intact porcine hearts at days 0, 3, 5 and 7 for all 4 decellularization conditions. Images are 1024 x 1024 pixels and 230 μm x 230 μm. N=8 images per condition were used for image analysis and statistics. Scale bar 50 μm.

MPM and ICS analysis of collagen and elastin microstructure

ICS analysis of the SHG images demonstrated quantitative differences in collagen microstructure amongst the decellularization conditions (Fig. 1.6). A_{SHG} increased in three of the four decellularization protocols, the exception was Trit Only in which A_{SHG} was approximately constant (Fig. 1.6A). In contrast, the R_{SHG} increased significantly in the two conditions characterized by loss of collagen crimping (Decell 3/4 and Tryp Only). ICS analysis of the TPF images revealed quantitative differences in elastin structure between the decellularization conditions: R_{TPF} decreased in Decell 3/4, Decell 1/6 and Tryp Only. In contrast, the R_{TPF} of Trit Only increased significantly characterized by retention of densely packed elastin fibers (Fig. 1.5).

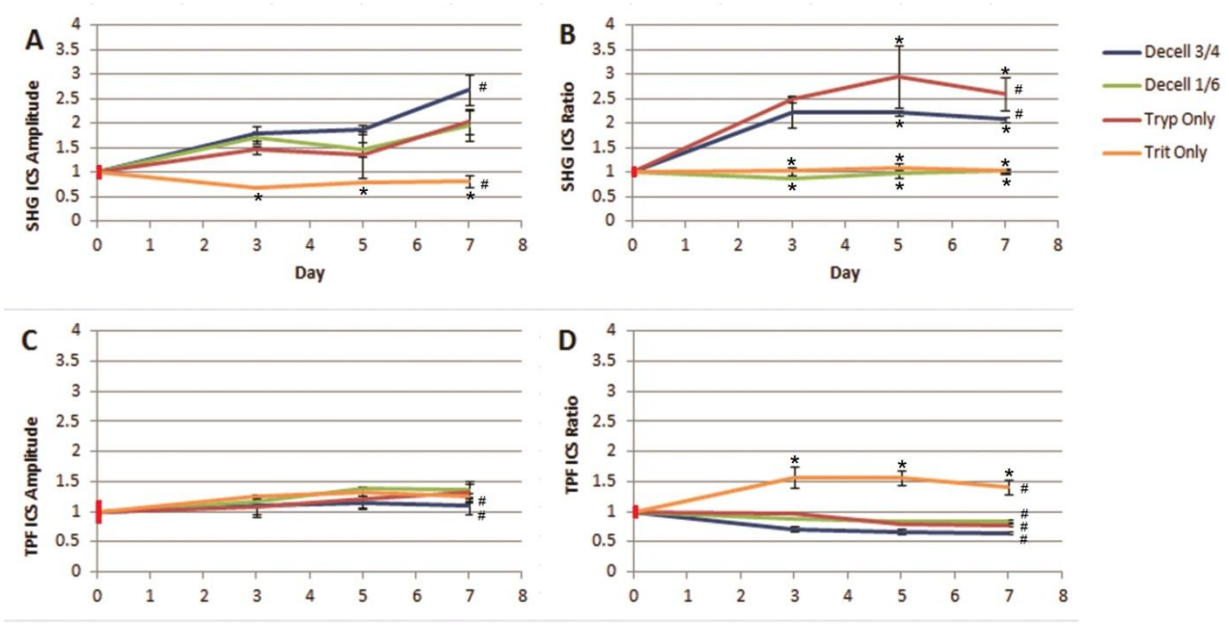

Figure 1.6. ICS of SHG and TPF. A) SHG ICS amplitude, B) SHG ICS ratio, C) TPF ICS amplitude, and D) ICS ratio were calculated from SHG and TPF images of intact porcine hearts at days 0, 3, 5 and 7 for all 4 decellularization conditions and normalized to day 0. Baseline SHG ICS amplitude for intact samples were 0.12, 0.11, 0.15, 0.13, respectively.

Baseline SHG ICS ratio for intact samples were 1.50, 1.65, 1.23, 1.23, respectively. Error bars at day 0 (in red) denote standard deviation of baseline values, normalized to the average baseline value (calculated separately for each condition). Error bars for subsequent days (in black) denote standard deviation of the normalized values. Asterisks represent statistically significant differences between conditions for that day (*$p < 0.05$). Number signs represent statistical variation with time for that condition ($p < 0.05$).

Mechanical properties correlate with ICS Amplitude and Ratio

ICS image analysis of the C-ECM during the decellularization process was compared to direct mechanical testing and protein assays. A_{SHG} modestly correlated with compressive modulus ($R^2 = 0.57$) and collagen content ($R^2 = 0.48$). However, there was a strong linear relationship between the log of A_{SHG} ($R^2 = 0.86$) and the log of the compressive modulus (Fig. 1.7A). R_{TPF} also strongly correlated with compressive modulus ($R^2 = 0.92$). However, A_{TPF} ($R^2 = .13$) and R_{SHG} ($R^2 = 0.34$) showed little correlation with compressive modulus. Backward stepwise elimination based on Akaike information criterion (AIC) showed the best variables predict E were A_{SHG} and R_{TPF} (AIC, 398): $E = 73.9*\text{Log}(A_{SHG}) + 70.1* R_{TPF} - 131$. This improved the fit to experimental data (R^2=0.94). In contrast, the AIC for the best single parameter (R_{TPF}) was 418. Thus by introducing one more variable (A_{SHG}), AIC improved by 20 (or 5%).

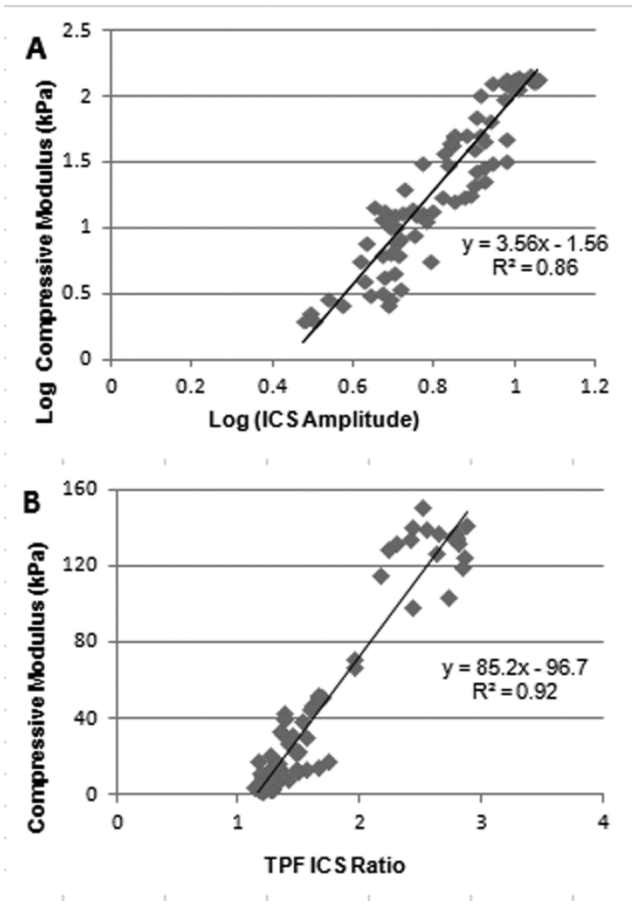

Figure 1.7. Relationship between Mechanical and Optical Properties. A) Scaling relationship for compressive modulus and ICS amplitude from SHG images and B) compressive modulus and ICS ratio from TPF images for all four decellularization conditions.

Discussion

Decellularization of the heart is a rapidly developing field that promises to create a scaffold for functional cardiac tissue engineering (21, 48, 58). However, the decellularization process impacts the ECM, and a non-invasive, non-destructive method to assess the C-ECM,

in particular the mechanical properties, has not yet been presented. We have demonstrated that MPM (SHG from fibrillar collagen and TPF from elastin) imaging of the C-ECM and ICS analysis provides quantitative and objective information about the C-ECM in a non-invasive and non-destructive fashion that can predict the compressive modulus of the decellularized matrix.

Variability in microstructure/mechanics between decellularization conditions.

It is perhaps important to first note that gross visual inspection of the C-ECM cannot distinguish between the decellularization protocols (Fig. 1.2). Thus, alternate methods are necessary to determine the extent of decellularization and changes to structural or mechanical properties. The most striking difference in the mechanical property amongst the decellularization conditions was the observation that Trit Only caused a significant increase in the compressive modulus while the remaining three conditions all caused a significant decrease. There are several factors potentially responsible for this observation. Despite a decrease in overall elastin content in all four conditions, TPF showed that Trit Only was the only condition to preserve the fibrillar nature of the elastin network (Fig. 1.5), although the density of the elastin fibers increased. The increased density of elastin could contribute to the increase in the compressive modulus. SHG also revealed a more densely crimped collagen structure of Trit Only, which could enhance the compressive modulus. This feature was reflected in the unique combination of a constant A_{SHG}, but an increase in R_{SHG}. Constant A_{SHG} suggests that collagen density did not change, while increased R_{SHG} instead shows a change in collagen fiber orientation. Finally the mechanism by which each reagent disrupts cells may also be a factor. Triton lyses cells by disrupting the cell

membrane and, unlike Trypsin, did not break the cell-ECM bonds. This may result in significant cell residue (not DNA) that could impact the compressive modulus.

Despite the near complete removal of cellular DNA (comparable to previously published results)(48), Decell 1/6 preserved collagen crimping, a feature of the native ECM, while Decell 3/4 did not. The C-ECM with crimped collagen fibers had a two-fold higher compressive modulus compared to the uncrimped C-ECM (5.8 kPa vs. 2.4 kPa, $p < 0.01$). These are physiologically relevant differences in compressive modulus (between 1 and 15kPa) (51, 52). During embryonic development, the passive modulus of cardiac tissue is approximately 3-4 kPa while the modulus of tissue surrounding the myocardium ranges from 9-14 kPa (64). The prolonged exposure to Trypsin likely disrupted collagen and elastin protein fibrils leading to a loss of fiber density (Fig. 1.5).

While C-ECM from Decell 3/4 and Decell 1/6 had different compressive moduli and collagen ultrastructure, they had similar levels of collagen content. This suggests that the presence of crimping in Decell 1/6 C-ECM may have been partly responsible for the higher compressive modulus. The increased compressive modulus of Trit Only and its preservation of elastin fibers (Fig. 1.5) also suggest that the presence of elastin may have played an important role in mechanical properties in C-ECM.

ICS amplitude and ICS ratio predict structure and mechanical properties.

Previous work has shown that ICS parameters correlate with fiber properties such as width, density and pore size (56, 61). However, additional properties, such as collagen

crimping or elastin content, will likely affect bulk mechanical properties. Expanding ICS analysis to include these additional features will help further define the relationship between ICS and bulk mechanical properties in natural tissues.

In our study, A_{SHG} and R_{TPF} correlated well with compressive modulus, and R_{SHG} appeared to increase with loss of collagen crimping. Logistic regression and backward stepwise elimination based on Akaike information criterion (AIC) showed the variables to predict compressive modulus were A_{SHG} and R_{TPF}, which improved the fit to experimental data (R^2=0.94) relative to a single variable (R_{TPF}). By introducing one more variable (A_{SHG}), AIC improved by 20 (or 5%). A_{TPF} (R^2 = .13) and R_{SHG} (R^2 = .34) showed almost no correlation with compressive modulus and were therefore excluded. The high degree of fit suggests that MPM and ICS provide a non-invasive means to determine structure and mechanical properties of C-ECM.

ICS amplitude has previously been shown to be inversely proportional to fiber density (62). Thus, our observed increase in A_{SHG} and A_{TPF} is likely a result of decreased collagen and elastin fiber density, confirmed by the protein assays that demonstrated a loss of total collagen and elastin content. However, another factor is the presence of light scatterers, including cells, during the early stages of decellularization. Cells scatter photons and reduce the MPM signal (59). Complete removal of cells results in sharper images of the SHG collagen structure and the TPF elastin structure. Thus, both loss of collagen and cells may have contributed to the observed increase in ICS amplitude.

Optimal decellularization for mechanical endpoints

Previous studies suggest an optimal ECM stiffness range for cardiomyocyte and cardiac fibroblast cell function exists (51, 52, 65). Stiffness significantly affects maturation and differentiation of immature ventricular myocytes, development of aligned sarcomeres, and generation of contractile force (51). Cardiomyocytes are also more likely to beat, and beat with greater frequency, when cultured on softer collagen gels with heart-like elasticity (52, 53). ECM mechanical properties also play a dominant role in maintaining fibroblast quiescence (65). As artificial substrate stiffness increases from that of normal parenchymal tissue (~10 kPa) to that of fibrotic, collagen-rich tissue (35-70 kPa), cultured fibroblasts transition from quiescence to a state of increased proliferation and matrix synthesis, suggesting that controlling ECM stiffness promotes cell functionality.

Previous work investigating the recellularization of C-ECM using cardiac, endothelial, fibroblast and stem cells had shown that the scaffold's architecture and composition promote cell functionality. Recellularization of decellularized rat hearts with cardiac and endothelial cells, with subsequent electrical and mechanical stimulation, create contractile tissues (21). Decellularized porcine hearts recellularized with cardiomyocytes support formation of organized cardiomyocyte sarcomeres (48), and have been shown to beat and express typical cardiac cell markers within a few days of seeding (49). This suggests that retaining ECM architecture and composition during decellularization will promote cell function upon recellularization.

Despite the current success in recellularizing natural and artificial scaffolds, the effect of collagen structure on cell fate remains relatively unexplored. A mechanical environment and structure similar to that of native myocardium should be most favorable. When comparing our two decellularization conditions, Decell 1/6 produced a compressive modulus and structure more similar to native extracellular matrix (42.4 kPa) relative to Decell 3/4 (5.8 kPa vs. 2.4 kPa). Additionally, Decell 3/4 appeared to damage collagen structure and compromise mechanical integrity, as seen by the loss of crimping and decrease in fiber density. This suggests that Decell 1/6 would be the preferred decellularization condition for maintaining cell function. Tryp Only and Trit Only were not valid decellularization techniques, as DNA loss was incomplete. Nonetheless, these conditions provide information about the affect each individual reagent has on collagen structure during the decellularization process. Trypsin severely reduced structure and mechanical integrity while Triton preserved the collagen crimping and increased the matrix stiffness. Our results emphasize the importance of appropriate timing when optimizing a decellularization protocol using these two reagents.

Conclusion

Decellularization of xenogeneic hearts potentially offers instructive matrix that may facilitate the development of engineered human heart tissue. Studies have shown that mechanical properties of the extracellular matrix can strongly influence cell response; however, the decellularization process impacts the C-ECM structural and mechanical properties. We have presented a non-invasive, non-destructive method to assess the

mechanical properties of the matrix that employs MPM imaging and ICS analysis. This process allows one to quantitatively assess the microstructure, and estimate the compressive modulus without compromising the C-ECM.

CHAPTER 2: Differential β_3 Integrin Expression Regulates the Response of Human Lung and Cardiac Fibroblasts to Extracellular Matrix and Its Components

Abstract

Extracellular matrix (ECM) derived from whole organ decellularization offers an instructive, 3D scaffold that may aid in the development of engineered tissues. However, decellularization disrupts the mechanical properties and protein composition of the ECM. Furthermore, fibroblast phenotype can be tissue-specific. We hypothesized that ECM structure and composition, fibroblast source, and integrin expression will influence fibroblast phenotype. Human cardiac fibroblasts (HCFs) and normal human lung fibroblasts (NHLFs) were cultured on cardiac ECM, lung ECM, and their individual components for 48 hours. COL1A expression of HCFs and NHLFs cultured on ECM and fibronectin coatings decreased to <50% of that of untreated cells; COL1A expression was 1-2-fold higher for HCFs cultured on stiffer substrates. NHLFs cultured on ECM and fibronectin coatings expressed 12-31-fold more alpha smooth muscle actin (α-SMA) than HCFs; the α-SMA expression was ~2-5 fold higher for HCFs and NHLFs cultured on stiffer substrates. HCFs expressed significantly higher levels of β_3, β_4 and $\alpha_v\beta_3$ integrins when compared to NHLFs. Inhibition of the β_3 integrin resulted in a 16-26-fold increase in α-SMA expression in HCFs cultured on ECM and fibronectin. This suggests that β_3 integrin expression is dictated primarily by the source of the fibroblast, and that its expression inhibits α-SMA expression (and thus the myofibroblast phenotype). We conclude that

substrate stiffness, fibroblast source, and integrin expression play important regulating fibroblast phenotype.

Introduction

Extracellular matrix (ECM) derived from whole organ decellularization offers a promising biological scaffold for tissue engineering applications. The native 3D structure and biochemical composition of these matrices must be able to support tissue-specific recellularization strategies. However, decellularization protocols use reagents that can disrupt the ECM resulting in a range of mechanical properties and protein composition that no longer reflect the ECM *in vivo* (29). Furthermore, fibroblast phenotype can be organ-specific (66). Thus, we may be able to improve the decellularization and recellularization process by identifying structural and biochemical features of the ECM that impact organ-specific fibroblast behavior.

Recellularization of decellularized matrices is an intriguing strategy to specifically engineer lung and cardiac tissue (21, 23) that will likely include stromal cells, such as the fibroblast. The fibroblast is an ubiquitous cell (e.g., it is the most numerous cell type in the heart) that plays a prominent role in the maintenance of tissue architecture through deposition of new, or remodeling of existing, ECM proteins. However, fibroblast cell response to the decellularized matrix remains relatively unexplored (21, 48, 49). Excessive contractile function or collagen deposition induced by abnormal mechanical properties or soluble

growth factors could interfere with normal structure and function of the recellularized tissue (67).

Integrins are membrane-bound proteins that play a critical role in ECM maintenance and remodeling by transmitting signals from the ECM to regulate cell function. In the case of the fibroblast, integrin expression can influence the expression of intracellular structural or contractile proteins such as alpha smooth muscle actin (α-SMA) (68), and thus the myofibroblast phenotype, as well as extracellular structural proteins such as collagen (69). However, previous work has not determined the effect of specific decellularized matrix features on fibroblast function and integrin signaling. For example, it is not well understood how collagen microstructure may affect α-SMA expression.

Finally, previous work has shown that fibroblast source can significantly affect cell morphology and ECM deposition (70). Similarly, ECM has been shown to influence chemotaxis, direct cell differentiation, and induce constructive host tissue remodeling responses (71). Nonetheless, it is still unclear whether fibroblast source or ECM structure and composition both impact fibroblast, and what role integrins may play in this process.

The goal of this study is to determine the effect of ECM structure and composition, fibroblast source, and integrin expression on fibroblast phenotype by seeding human cardiac and lung fibroblasts on cardiac ECM, lung ECM, and their individual components. Our results demonstrate that β_3 integrin expression is dictated primarily by the source of the fibroblast, and that its expression inhibits α-SMA expression (and thus the

myofibroblast phenotype). This result suggests that organ-specific fibroblasts may be an important factor in effective recellularization strategies.

Materials and Methods

Cell culture

Human cardiac fibroblasts (HCFs) and normal human lung fibroblasts (NHLFs) were independently seeded at a density of 3,500 cells/cm^2 on T-25 tissue culture flasks coated for 1 hour at 37 C with 1mg/mL type I collagen (coll coat), 25µg/mL fibronectin (FN coat), 1mg/mL C-ECM (CECM1 coat, CECM2 coat and CECM3 coat) or 1mg/mL L-ECM (LECM1 coat), as well as on T-25 flasks containing 2 mL collagen gels (coll gel) or intact C-ECM samples (CECM2 intact and CECM3 intact). Cells were also seeded on uncoated flasks that were left untreated (by which our data was normalized to), or treated with 50ng/mL TGF-β or 100ng/mL TNF-α (N=3, Table 2.1).

Preparation of ECM

Whole porcine hearts were obtained immediately after euthanasia of 40–55 kg, adult female Yorkshire pigs. The excess fat and connective tissue were removed, and the coronaries were perfused with phosphate-buffered saline to remove coagulated blood. Each heart was frozen at - 80 C for at least 24 hours to aid in cell lysis. These hearts were then thawed at room temperature and decellularized over a 7-day period by coronary perfusion with two different solutions of either Trypsin/EDTA/NaN_3 and

Triton/EDTA/NaN_3 as previously described (48). Different combinations of Trypsin and Triton were used as their mechanism of action should differentially impact the ECM (48, 58). Full-thickness left ventricular tissue samples (1 x 1 cm) were collected after 7 days (CECM2 intact and CECM3 intact). The decellularized C-ECM was then desiccated and reduced to a powder. One gram of C-ECM powder and 100 mg of pepsin (Sigma, ~2,500 U/mg) were mixed in 100 mL of 0.01M HCl and mixed for 4 days at room temperature. The resulting solution had a pH of approximately 2.8-3.2. C-ECM coatings were formed by mixing 0.1M NaOH and 1x PBS at 4 C. The solution was brought to 1 mg/mL and pH 8.5 and then coated on T-25 flasks for 1 hour at 37 C (CECM2 coat and CECM3 coat). C-ECM and L-ECM was also provided by the Christman lab (CECM1 coat and LECM1 coat) and prepared as previously described (72). Briefly, porcine ventricular tissue and lung tissue was decellularized using 1% sodium docecyl sulfate for 4-5 days. The decellularized ECM was then rinsed with Triton X-100 for 30 min and with deionized water overnight, and milled into a fine powder. The powder was then digested in pepsin in 0.1M HCl.

RNA quantification

Total RNA was isolated from HCFs and NHLFs after 48 hours of culture under each condition (Aurum Total RNA Mini Kit and RNAzol). RNA quantity and purity were measured using a spectrophotometer (DU 730 Beckman Coulter). cDNA was then synthesized from mRNA (iScript Reverse Transcription Supermix). An optimal reference gene was then chosen using a commercially available pre-designed plate (Reference Gene H96). Type 1 collagen (COL1A, FIG 2.1), α-smooth muscle actin (α-SMA, FIG 2.1) and glucose-6-phosphate dehydrogenase (G6PD) RNAs were then quantified by Real Time

Quantitative PCR (PrimePCR SYBR Green Assay) using a CFX96 Real Time PCR Detection System (Biorad). A standard curve was created for each primer using 2-fold serially diluted cDNA from untreated HCFs and NHLFs. From these curves, gene expression was determined for each condition relative to untreated cells. The target genes' (COL1A and α-SMA) expression was then quantified relative to the housekeeper gene (G6PD) for each condition, to account for differences in cell proliferation.

Integrin expression quantification

HCF and NHLF cell suspensions were prepared by rinsing each condition (collagen, L-ECM, C-ECM and fibronectin coatings) with HBSS, and then treating each flask with 0.025% Trypsin in PBS for 4 minutes. Cells were then resuspended in assay buffer and added to integrin assay wells at 100,000 cells/well (per manufacturer's instructions, Alpha/Beta Integrin-Mediated Cell Adhesion Array Combo Kit). Each well was used to capture cells expressing particular integrins on their cell surface. Unbound cells were washed away, and adherent cells were fixed and stained. Relative cell attachment was determined using absorbance readings, measured at 540nm using a Bio-Rad Benchmark Microplate Reader (FIG 2.2).

Functional blocking studies

In inhibition studies with blocking antibodies (FIG 2.3), HCF and NHLF cell suspensions were treated with 10μg/mL of anti-β3-integrin (CD61, Millipore) or 10μg/mL of anti-β4-integrin (ASC-8, Millipore) for 30 minutes and then seeded on T25 tissue culture flasks as previously described.

α-SMA Staining

HCFs and NHLFs were stained with a monoclonal antibody recognizing α-SMA followed by AlexaFluor488 goat anti-mouse IgG. Samples were counterstained with DAPI to visualize cell nuclei and analyzed using confocal microscopy (FIG 2.4). Area fraction of the regions stained by α-SMA was measured from thresholded images using ImageJ.

Mechanical testing

The compressive modulus of collagen gels and intact C-ECM samples were measured (FIG 2.5) via indentation testing (Synergie 100; MTS Systems Corporation). The sample height (15mm) was measured using a linear extensor. Each sample was then compressed to 20% strain with a 5-mm radius plate at a rate of 0.02 mm/s. Data were acquired with a 10N load cell at 50 Hz with a 12 bit data acquisition. The modulus was calculated in the linear region of the stress–strain curve. Each sample was tested in five locations and the values averaged.

Statistical analysis

The COL1A RNA content, α-SMA RNA content, integrin expression, compressive modulus and promoter reporter fluorescence were analyzed using one-way ANOVA and paired t-tests. SigmaStat was used to perform the statistical tests ($p < 0.05$).

Results

COL1A RNA content

Culture of HCFs and NHLFs on ECM and fibronectin coatings decreased the COL1A expression to <50% of that of untreated cells. In contrast, collagen coatings had no significant effect on COL1A expression. For the cells treated with TGF-β as a positive control, HCF COL1A expression increased by 1.15-fold and NHLF COL1A expression increased by ~15-fold. For the cells treated with TNF-α as a negative control, HCF COL1A expression decreased by 36% and NHLF COL1A expression decreased by 29%. These changes in expression agree with other published findings describing the effects of TGF-β and TNF-α on collagen production (73-76).

Culture of HCFs on stiffer substrates resulted in increased COL1A expression, while NHLFs had mixed results. HCFs cultured on collagen coatings had a 1.38-fold higher COL1A expression than HCFs cultured on collagen gels (1.07 vs. 0.45, $p<0.01$). HCFs cultured on CECM2 coatings had a twofold higher COL1A expression than HCFs cultured on CECM2 intact samples (0.30 vs. 0.10, $p<0.01$). Similarly, NHLFs cultured on collagen coatings had a 100% higher COL1A expression than NHLFs cultured on collagen gels (1.03 vs. 0.50, $p<0.01$). However, NHLFs cultured on CECM3 coatings showed the opposite trend, and had 63% lower COL1A expression than NHLFs cultured on CECM3 intact samples (0.30 vs. 0.82, $p<0.01$). Culture of NHLFs on CECM2 coatings and CECM2 intact samples did not show a significant difference in COL1A expression.

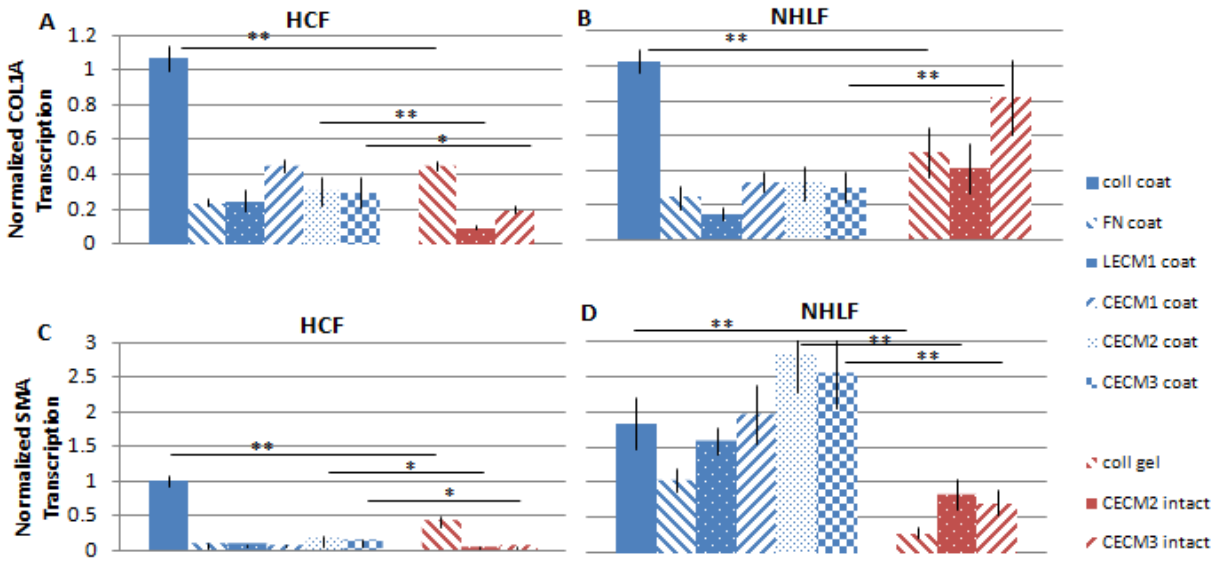

FIG 2.1: COL1A and α-SMA RNA Content of HCFs and NHLFs quantified by RT-qPCR and normalized to expression of untreated fibroblasts. Asterisks represent statistically significant differences between conditions (*p < 0.05, **p < 0.01).

α-SMA RNA content

NHLFs cultured on ECM and fibronectin coatings expressed significantly more α-SMA than HCFs cultured under the same conditions (12-31 fold more α-SMA expressed by NHLFs compared to HCFs). Culture of HCFs on ECM and fibronectin coatings decreased α-SMA expression to <15% of that of untreated HCFs. In contrast, collagen coatings had no significant effect on α-SMA expression of HCFs. NHLFs cultured on ECM and collagen coatings increased α-SMA expression by 59-182%. In contrast, fibronectin coatings had no significant effect on α-SMA expression of NHLFs. For the cells treated with TGF-β as a positive control, HCF α-SMA expression increased by 71% and NHLF α-SMA expression increased by ~29-fold. For the cells treated with TNF-α as a negative control, HCF α-SMA expression decreased by 36% and NHLF α-SMA expression decreased by 28%. These

changes in expression agree with other published findings describing the effects of TGF-β and TNF-α on α-SMA production (77-79).

Culture of HCFs and NHLFs on stiffer substrates resulted in increased α-SMA expression. α-SMA expression of HCFs was 1.43-fold higher for collagen coatings than for collagen gels (1.02 vs. 0.42, $p<0.01$), 2.75-fold higher for CECM2 coatings than for CECM2 intact samples (0.15 vs. 0.04, $p<0.05$) and 1.4-fold higher for CECM3 coatings than for CECM3 intact samples (0.12 vs. 0.05, $p<0.05$). Likewise, α-SMA expression of NHLFs was 5.3-fold higher for collagen coatings than for collagen gels (1.83 vs. 0.29, $p<0.01$), 2.37-fold higher for CECM2 coatings than for CECM2 intact samples (2.83 vs. 0.84, $p<0.01$) and 2.53-fold higher for CECM3 coatings than for CECM3 intact samples (2.54 vs. 0.72, $p<0.01$).

α/β surface integrin expression

HCFs expressed similar α and β integrin levels when cultured on collagen, fibronectin, L-ECM or C-ECM coatings, with the exception of HCF expression of α_4 integrin on fibronectin which decreased significantly when compared to α_4 expression on other substrates. Likewise, NHLFs expressed similar integrin levels when cultured on these four coatings. Both NHLFs and HCFs expressed low levels of β_2 and β_6; however, their expression of β_3 and β_4 was markedly different. While NHLFs expressed very low levels of β_3, β_4 and $\alpha_v\beta_3$ integrins (mean±SD of 0.05±0.03, 0.04±0.02 and 0.32±0.07, respectively), HCFs showed a significantly higher expression of these integrins (0.33±0.05, 0.27±0.16 and 0.80±0.23, respectively).

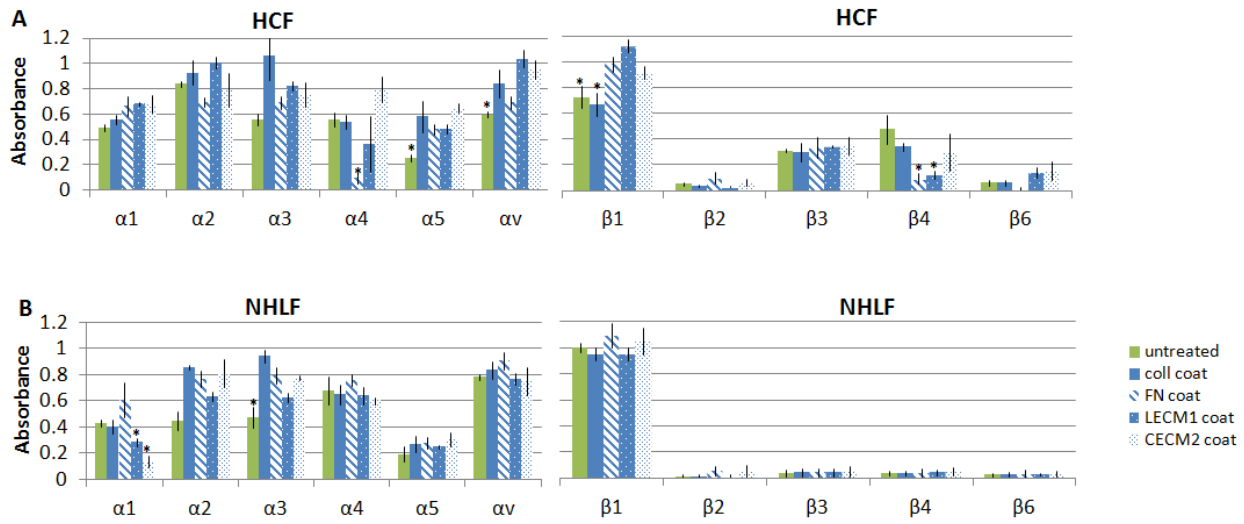

FIG 2.2: α/ β Integrin Expression of HCFs and NHLFs. Asterisks represent statistically significant differences between conditions (*p < 0.05).

Inhibition of β_3 and β_4 Integrins

Because the expression of β_3 and β_4 was markedly different between NHLFs and HCFs, as well as the expression of α-SMA, we sought to determine whether there was a link. Inhibition of the β_3 integrin did not significantly impact COL1A expression in HCFs and NHLFs, nor did inhibition impact α-SMA expression in NHLFs. In contrast, inhibition of the β_3 integrin dramatically increased α-SMA expression of HCFs cultured on fibronectin (16-fold) and ECM (20-26-fold). Inhibition of the β_4 integrin had no significant effect on COL1A and α-SMA expression in either HCFs or NHLFs.

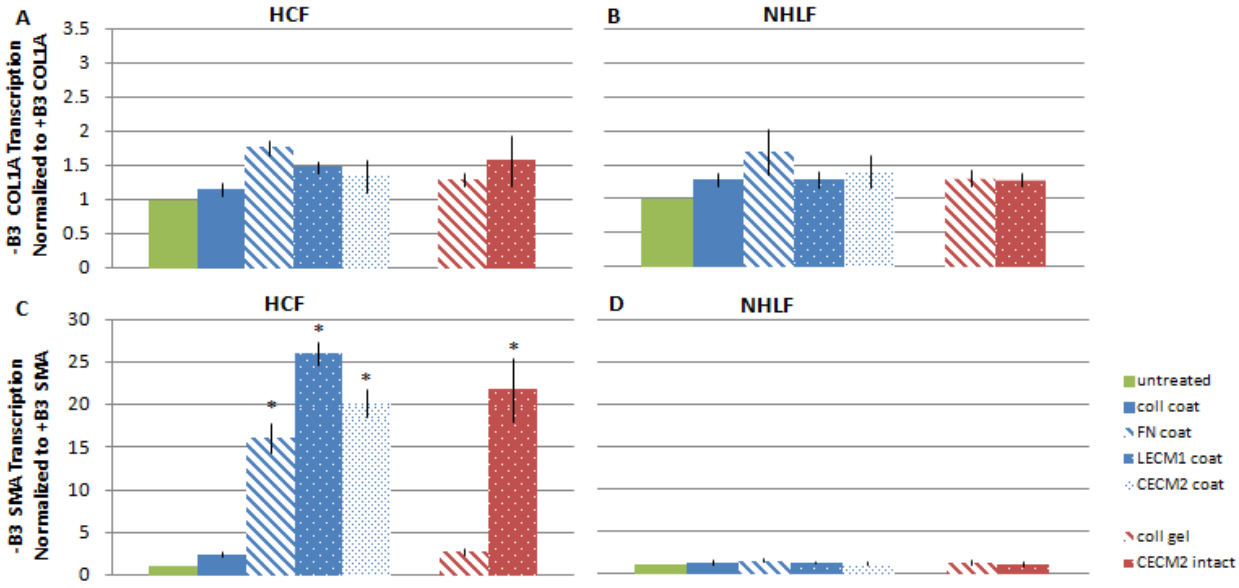

FIG 2.3a: COL1A and α-SMA RNA content of HCFs and NHLFs with 48hr incubation with β_3 integrin blocking antibodies (**-B3**) normalized to RNA content of NHLFs and HCFs without integrin blocking antibodies (**+B3**). Asterisks represent statistically significant differences between conditions (*$p < 0.05$).

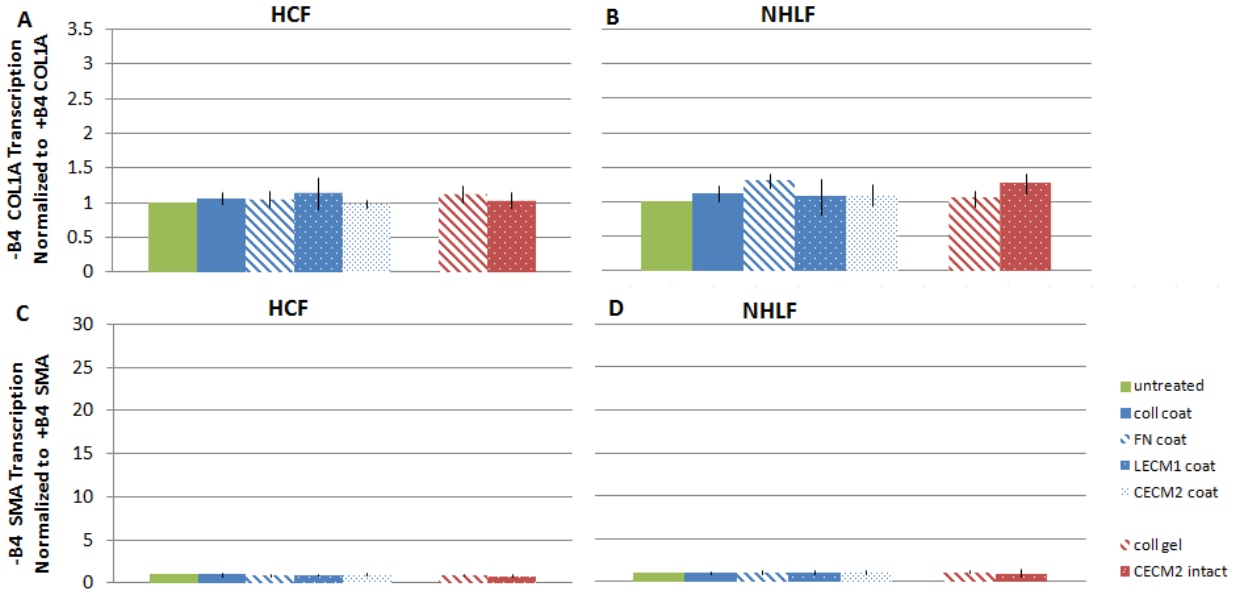

FIG 2.3b: COL1A and α-SMA RNA content of HCFs and NHLFs with 48hr incubation with β_4 integrin blocking antibodies (**-B4**) normalized to RNA content of NHLFs and HCFs without integrin blocking antibodies (**+B4**).

α-SMA staining

α-SMA staining revealed increased levels of α-SMA proteins in untreated NHLFs compared to untreated HCFs (area fraction of 4.96% compared to 0.41%). Inhibition of the β_3 integrin in HCFs cultured on CECM2 coatings resulted in a significant increase in α-SMA compared to non-inhibited HCFs (area fraction of 2.54% compared to 0.03%).

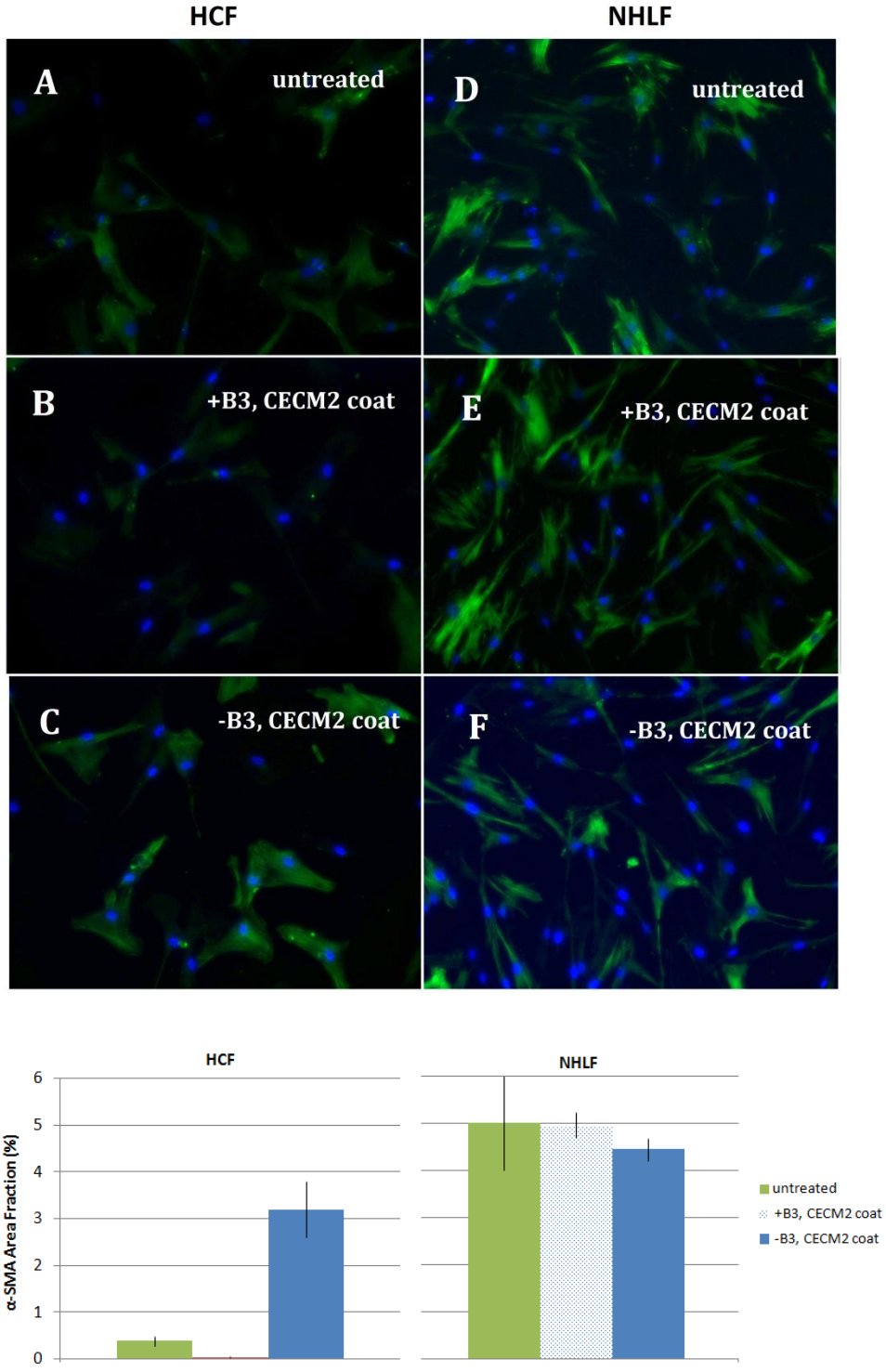

FIG 2.4: Detection of α-SMA (green) in HCFs (top row) and NHLFs (bottom row) with and without 48hr incubation with β_3 integrin blocking antibodies.

Mechanical properties

Compressive modulus of each coating was comparable to uncoated polystyrene (~3GPa). The collagen gels, intact CECM2 and intact CECM3 samples had moduli several orders of magnitude lower (mean±SD of 1.34±0.23, 5.40±0.94 and 2.42±0.40kPa, respectively).

Discussion

Whole organ decellularization is a rapidly developing field that offers instructive ECM that may aid in the development of engineered tissues. However, decellularization impacts the mechanical properties and protein composition of the ECM (29), and organ-specific fibroblast cell response to the decellularized matrix has not been described. Since lung and heart are two organs that have received significant attention in the literature describing decellularized organs (21-23, 49), we determined the response of lung and cardiac fibroblasts to a series of different substrates including organ-specific decellularized ECM and their specific sub-components. Our results demonstrate that substrate stiffness and cell source (as opposed to the organ-specific ECM) are the primary determinants impacting fibroblast phenotype (i.e., myofibroblast). In particular, β_3 integrin expression is significantly higher in HCFs, and this directly inhibits α-SMA expression, and thus the myofibroblast phenotype.

Substrate stiffness regulates the fibrotic response

Decellularization significantly reduces the mechanical properties of the ECM such that it no longer reflects the mechanical properties of the ECM *in vivo*. HCFs and NHLFs cultured on the decellularized ECM and collagen coatings resulted in increased COL1A and α-SMA expression, when compared to the intact decellularized ECM and collagen gels. Since the protein composition of the coating and the intact decellularized ECM are identical, we conclude that culture of fibroblasts on stiffer substrates results in a myofibroblast phenotype and an increased fibrotic response. Previous studies have shown that the mechanical properties of a cell's microenvironment have as significant an impact on cell morphology and function as soluble factors and cell-cell contact (80, 81). Cells cultured on stiff substrates upregulate the expression of integrins (37), assemble actin stress fibers (82), and exhibit a more spread phenotype (80). Cells cultured on coated flasks are likely responding to the stiffness of the polystyrene. Our findings are consistent with these previous reports. Of particular interest is that these findings suggest that HCFs and NHLFs will generally express less α-SMA and produce less collagen if introduced directly into decellularized ECM which is mechanically softer than intact tissue.

Differential response of human cardiac and lung fibroblasts to decellularized ECM

NHLFs cultured on ECM and fibronectin coatings expressed significantly more α-SMA than HCFs cultured under the same conditions. The higher expression of α-SMA expression in NHLFs typifies a myofibroblast or activated phenotype, in comparison to the quiescent HCFs. This suggests that NHLFs will be more contractile, more migratory and more likely to deposit ECM proteins than HCFs (83-85). Several types of cells have been used to recellularize ECM, with varying levels of success, including smooth muscle, endothelial, and

fibroblast (22, 49, 86). However, few comparative studies have been performed to determine potential benefits of using tissue-specific cells to recellularize ECM. Here, we see that organ specific stromal cells have intrinsic differences in protein expression (i.e., α-SMA) that may profoundly influence cell response during recellularization.

Differential integrin expression of cardiac and lung fibroblasts

We hypothesized that the differential expression of α-SMA by the lung and cardiac fibroblasts might be due to differences in the expression of cell surface integrins as these proteins interact directly with ECM proteins to impact protein expression and cell function such as migration (68, 69, 87). In general, we found that the choice of ECM coating did not impact integrin expression; rather, we found significant differences in the expression of integrin β_3 and β_4 between the lung and cardiac fibroblast.

Integrins are membrane-bound proteins that mediate cell-cell and cell-ECM interactions. They play a critical role in ECM maintenance and remodeling by transmitting signals from the ECM to regulate cell function. The β_3 subunit, most commonly associated with α_v, has been shown to regulate wound healing and re-epithelialization (69). Expression of $\alpha_v\beta_3$ (a receptor for vitronectin and other ECM molecules) is elevated on several cell types involved in wound healing, including dermal fibroblasts. $\alpha_v\beta_3$ has been shown to regulate fibroblast phenotype, TGF-β receptor expression, and downstream TGF-β signaling. β_4 integrin subunits are usually found in $\alpha_6\beta_4$, an integrin laminin receptor. $\alpha_6\beta_4$ has been reported to play important roles in epithelial cell migration by mediating traction forces and signaling molecules.

Expression of integrin β_3 inhibits α-SMA expression

Higher levels of β_3 and β_4 integrins in HCFs, combined with their role in wound healing and cell migration, suggested that they may play a role in suppressing the expression of α-SMA. Functional blocking antibodies against β_3 integrins, but not β_4, in HCFs significantly increased α-SMA expression. Staining confirmed significantly higher α-SMA expression in HCFs after blocking the β_3 integrin. This result demonstrates that β_3 expression can regulate α-SMA expression, and thus the myofibroblast phenotype. In addition, this result suggests that tissue-specific fibroblasts may play an important role in organ-specific recellularization strategies.

Fibroblast expression of COL1A and α-SMA has previously been shown to be strongly associated, resulting from myofibroblast differentiation and the fibrotic response (85, 88, 89). However, we did not observe a correlation between COL1A and α-SMA in our study. In particular, COL1A expression was generally not higher in NHLFs cultured on stiffer substrates. This may have been due to the timescale of our experiments, since we measured COL1A and α-SMA expression 48 hours after seeding the fibroblasts. Longer time points may result in elevated COL1A. There may have also been other factors mediating COL1A expression beyond mechanical properties, such as structural features of the ECM. We previously demonstrated that different decellularization conditions can produce ECM with significantly different collagen and elastin structures (29). These structural features may play a role in regulating COL1A and α-SMA expression.

Conclusion

Whole organ decellularization potentially offers an instructive matrix for the creation of engineered tissues. Studies have shown ECM can influence chemotaxis, direct cell differentiation and induce constructive host tissue remodeling; however, many decellularization protocols use damaging reagents, which produce ECM with a wide range of mechanical properties and protein composition. Our results demonstrate that in addition to substrate stiffness, the source of fibroblast can significantly impact phenotype, and that the differential response is linked to β_3 integrin expression. We conclude that substrate stiffness, cell source and β_3 integrin expression play important roles in controlling normal stromal cell function during recellularization.

CHAPTER 3: Summary and Conclusions

Tissue engineering whole organs using ECM derived from whole organ decellularization will potentially offer an alternative to allogeneic transplantation for patients suffering from end-stage organ failure. ECM provides an instructive matrix, with physical and chemical cues that can enhance cell functionality and viability. However, decellularization is a damaging process that results in loss of ECM structure, protein content and mechanical integrity. Several groups have derived ECM with a wide range of stiffnesses, which can subsequently impact cell response during recellularization. Despite the important roles substrate stiffness and composition play in regulating cell behavior, the impact of decellularization on ECM structure and mechanics is not well understood. By determining the relationship between ECM structure and mechanical properties, we can tailor decellularization protocols to enhance cell response during recellularization.

Imaging the structural proteins collagen and elastin will help improve our understanding of the relationship between ECM structure mechanical properties. In this work, we used MPM, combined with ICS, to non-invasively and non-destructively characterize structural and mechanical properties of the decellularized cardiac matrix. ICS amplitude of SHG collagen images and ICS ratio of TPF elastin images strongly correlated with compressive modulus. This showed that collagen fiber density and elastin fiber alignment dictate mechanical properties of the ECM.

MPM and ICS provide a method by which we can now non-invasively assess structural and mechanical changes in ECM during decellularization. This will enable groups to make real-time comparisons between ECM scaffolds from different decellularization protocols, without removal of tissue for testing. Leaving the ECM intact by using an optical method of assessment will allow for a greater number of measurements and minimize damage to the tissue. The structural changes that occur during the entire process of decellularization are not well understood. A more thorough understanding of the impact that each decellularization reagent has on the ECM will help optimize decellularization protocols for each organ system. Decellularization reagents have been shown to be damaging to the ECM structure, and we have shown that overexposure of tissue to Trypsin during decellularization can result in loss of collagen structure and mechanical integrity. Therefore, careful timing and choice of reagents is necessary to maintain ECM structure and mechanical properties.

Despite the continued progress in the field of whole organ recellularization since 2008, there remain many milestones that must be met before fully functional tissues can be created. Some of these milestones will require an improved understanding of cell-ECM interactions, such as fibrosis. Fibrosis has been shown to impact tissue function in recellularized ECM used as skin grafts, and it will likely present a challenge while recellularizing ECM for other organs. By studying the response of important stromal cell types such as fibroblasts to the ECM, we will be able to improve current recellularization strategies by optimizing cell-ECM interactions.

In this study, we cultured cardiac and lung fibroblasts on cardiac ECM, lung ECM and their components to determine the effect of substrate composition, tissue specificity and integrin expression on fibroblast phenotype. Collagen and α-SMA expression increased for stiffer substrates, and lung fibroblasts expressed significantly higher levels of α-SMA than cardiac fibroblasts. Higher expression of β_3 and β_4 integrins in cardiac fibroblasts suggested that integrin signaling may be responsible. Functional blocking antibodies against β_3 integrins increased α-SMA expression in cardiac fibroblasts, but had no effect on lung fibroblasts. This result demonstrates that β_3 plays an important role in regulating cardiac fibroblast phenotype.

We have demonstrated that both cell source and ECM can impact stromal cell response to ECM. Traditionally, a tissue specific ECM is believed to be most suitable for promoting cell behavior. Previous work has demonstrated that native ECM can enhance cell maturation and differentiation. However, we have shown that there may be exceptions when cells from another source are more appropriate for recellularizing a particular organ. In the case that a less contractile phenotype is desirable, a cardiac fibroblast may be more appropriate than lung fibroblast when recellularizing lung ECM. This concept can apply when choosing a source for any cell types, given that many cell types have shown to have source-specific phenotype and gene expression. Furthermore, we have identified integrin expression as being an important mechanism that can regulate source-specific fibroblast response. This has demonstrated that integrin expression can be used to help identify a desirable phenotype by screening for the presence of β_3 integrin, rather than directly testing all fibroblast-substrate combinations. However, integrin signaling is complex and there will

certainly be many non-integrin factors that regulate the cell response to ECM. Therefore, an improved understanding of integrin-mediated cell response to ECM will help identify integrins that can regulate cell phenotype.

We have presented a non-invasive, non-destructive method to assess the ECM structure and mechanical properties using MPM imaging and ICS analysis. Our findings show that ECM stiffness strongly correlates with collagen fiber density and elastin alignment in the ECM following decellularization, which can potentially impact fibroblast collagen and α-SMA expression during recellularization. Furthermore, differential expression of β_3 integrins in organ-specific fibroblasts impacts α-SMA expression suggesting that both stromal cell source and ECM structure can impact the remodeling response during recellularization.

A non-invasive method for assessing structural and mechanical changes in the ECM during decellularization will help make quantitative comparisons between different decellularization techniques and their effectiveness. By taking more measurements, non-destructively we can more accurately track the specific impact of each decellularization reagent. From this, decellularization protocols can be optimized to fit the needs of each organ system. Furthermore, the impact of substrate stiffness on fibroblast phenotype emphasizes the importance of careful timing during decellularization.

We also showed that fibroblast source played an equally important role in regulating cell response to the ECM. Source-specific differences in cell response demonstrate that there

can be advantages of using cells from a particular source to recellularize an organ. Source-specific fibroblast integrin expression also regulates cell phenotype, and may help identify cells with desirable characteristics.

Decellularization and recellularization of whole organs are promising solutions to help alleviate the need for donor organs. ECM recellularized with selected cell populations potentially offers an alternative to allogeneic transplantation for patients afflicted with end-stage organ failure. However, we are still far from recapitulating complex organ function. These constructs lack functionality, intact vascular networks and large animal studies are still required. Nevertheless, a tremendous amount of progress has been made since the creation of the first whole-heart construct in 2008.

REFERENCES

1. Lloyd-Jones, D., Adams, R.J., Brown, T.M., Carnethon, M., Dai, S., De Simone, G., Ferguson, T.B., Ford, E., Furie, K., Gillespie, C., Go, A., Greenlund, K., Haase, N., Hailpern, S., Ho, P.M., Howard, V., Kissela, B., Kittner, S., Lackland, D., Lisabeth, L., Marelli, A., McDermott, M.M., Meigs, J., Mozaffarian, D., Mussolino, M., Nichol, G., Roger, V.L., Rosamond, W., Sacco, R., Sorlie, P., Thom, T., Wasserthiel-Smoller, S., Wong, N.D., and Wylie-Rosett, J. Heart disease and stroke statistics--2010 update: a report from the American Heart Association. Circulation 121, e46, 2010.

2. Shin'oka, T., Imai, Y., and Ikada, Y. Transplantation of a tissue-engineered pulmonary artery. N Engl J Med 344, 532, 2001.

3. Go, A.S., Mozaffarian, D., Roger, V.L., Benjamin, E.J., Berry, J.D., Blaha, M.J., Dai, S., Ford, E.S., Fox, C.S., Franco, S., Fullerton, H.J., Gillespie, C., Hailpern, S.M., Heit, J.A., Howard, V.J., Huffman, M.D., Judd, S.E., Kissela, B.M., Kittner, S.J., Lackland, D.T., Lichtman, J.H., Lisabeth, L.D., Mackey, R.H., Magid, D.J., Marcus, G.M., Marelli, A., Matchar, D.B., McGuire, D.K., Mohler, E.R., 3rd, Moy, C.S., Mussolino, M.E., Neumar, R.W., Nichol, G., Pandey, D.K., Paynter, N.P., Reeves, M.J., Sorlie, P.D., Stein, J., Towfighi, A., Turan, T.N., Virani, S.S., Wong, N.D., Woo, D., and Turner, M.B. Heart disease and stroke statistics--2014 update: a report from the American Heart Association. Circulation 129, e28, 2014.

4. Minino, A.M., Murphy, S.L., Xu, J., and Kochanek, K.D. Deaths: final data for 2008. Natl Vital Stat Rep 59, 1, 2011.

5. Orens, J.B., and Garrity, E.R., Jr. General overview of lung transplantation and review of organ allocation. Proc Am Thorac Soc 6, 13, 2009.

6. Lee, S.J., and Atala, A. Scaffold technologies for controlling cell behavior in tissue engineering. Biomed Mater 8, 010201, 2013.

7. Fisher, M.B., and Mauck, R.L. Tissue engineering and regenerative medicine: recent innovations and the transition to translation. Tissue Eng Part B Rev 19, 1, 2013.

8. Liu, Y., Lim, J., and Teoh, S.H. Review: development of clinically relevant scaffolds for vascularised bone tissue engineering. Biotechnol Adv 31, 688, 2013.

9. Li, S., Sengupta, D., and Chien, S. Vascular tissue engineering: from in vitro to in situ. Wiley Interdiscip Rev Syst Biol Med 6, 61, 2014.

10. Stock, U.A., and Vacanti, J.P. Tissue engineering: current state and prospects. Annu Rev Med 52, 443, 2001.

11. Griffith, L.G., and Naughton, G. Tissue engineering--current challenges and expanding opportunities. Science 295, 1009, 2002.

12. Bottcher-Haberzeth, S., Biedermann, T., Klar, A.S., Pontiggia, L., Rac, J., Nadal, D., Schiestl, C., Reichmann, E., and Meuli, M. Tissue engineering of skin: human tonsil-derived mesenchymal cells can function as dermal fibroblasts. Pediatr Surg Int 30, 213, 2014.

13. Sloff, M., Simaioforidis, V., de Vries, R., Oosterwijk, E., and Feitz, W. Tissue Engineering of the Bladder: Reality or Myth? - a Systematic Review. J Urol, 2014.

14. Dunphy, S.E., Bratt, J.A., Akram, K.M., Forsyth, N.R., and El Haj, A.J. Hydrogels for lung tissue engineering: Biomechanical properties of thin collagen-elastin constructs. J Mech Behav Biomed Mater, 2014.

15. Georgiadis, V., Knight, R.A., Jayasinghe, S.N., and Stephanou, A. Cardiac tissue engineering: renewing the arsenal for the battle against heart disease. Integr Biol (Camb) 6, 111, 2014.

16. Sengupta, D., Waldman, S.D., and Li, S. From In Vitro to In Situ Tissue Engineering. Ann Biomed Eng, 2014.

17. Watson, C.J., Phelan, D., Collier, P., Horgan, S., Glezeva, N., Cooke, G., Xu, M., Ledwidge, M., McDonald, K., and Baugh, J.A. Extracellular matrix sub-types and mechanical stretch impact human cardiac fibroblast responses to transforming growth factor beta. Connect Tissue Res 55, 248, 2014.

18. Farzaneh, Z., Pakzad, M., Vosough, M., Pournasr, B., and Baharvand, H. Differentiation of human embryonic stem cells to hepatocyte-like cells on a new developed xeno-free extracellular matrix. Histochem Cell Biol, 2014.

19. Han, S.K., Kim, S.Y., Choi, R.J., Jeong, S.H., and Kim, W.K. Comparison of tissue-engineered and artificial dermis grafts after removal of basal cell carcinoma on face--a pilot study. Dermatol Surg 40, 460, 2014.

20. Lin, L., Zhu, J., Kottke-Marchant, K., and Marchant, R.E. Biomimetic-engineered poly (ethylene glycol) hydrogel for smooth muscle cell migration. Tissue Eng Part A 20, 864, 2014.

21. Ott, H.C., Matthiesen, T.S., Goh, S.K., Black, L.D., Kren, S.M., Netoff, T.I., and Taylor, D.A. Perfusion-decellularized matrix: using nature's platform to engineer a bioartificial heart. Nat Med 14, 213, 2008.

22. Ott, H.C., Clippinger, B., Conrad, C., Schuetz, C., Pomerantseva, I., Ikonomou, L., Kotton, D., and Vacanti, J.P. Regeneration and orthotopic transplantation of a bioartificial lung. Nat Med 16, 927, 2010.

23. Petersen, T.H., Calle, E.A., Zhao, L., Lee, E.J., Gui, L., Raredon, M.B., Gavrilov, K., Yi, T., Zhuang, Z.W., Breuer, C., Herzog, E., and Niklason, L.E. Tissue-engineered lungs for in vivo implantation. Science 329, 538, 2010.

24. Moran, E.C., Dhal, A., Vyas, D., Lanas, A., Soker, S., and Baptista, P.M. Whole-organ bioengineering: current tales of modern alchemy. Transl Res 163, 259, 2014.

25. Robertson, M.J., Dries-Devlin, J.L., Kren, S.M., Burchfield, J.S., and Taylor, D.A. Optimizing recellularization of whole decellularized heart extracellular matrix. PLoS One 9, e90406, 2014.

26. Tsuchiya, T., Sivarapatna, A., Rocco, K., Nanashima, A., Nagayasu, T., and Niklason, L.E. Future prospects for tissue engineered lung transplantation: Decellularization and recellularization-based whole lung regeneration. Organogenesis 10, 2014.

27. Keane, T.J., and Badylak, S.F. The host response to allogeneic and xenogeneic biological scaffold materials. J Tissue Eng Regen Med, 2014.

28. Badylak, S.F. Decellularized Allogeneic and Xenogeneic Tissue as a Bioscaffold for Regenerative Medicine: Factors that Influence the Host Response. Ann Biomed Eng, 2014.

29. Merna, N., Robertson, C., La, A., and George, S.C. Optical imaging predicts mechanical properties during decellularization of cardiac tissue. Tissue Eng Part C Methods 19, 802, 2013.

30. Tsuchiya, T., Balestrini, J.L., Mendez, J.J., Calle, E.A., Zhao, L., and Niklason, L. Influence of pH on Extracellular Matrix Preservation During Lung Decellularization. Tissue Eng Part C Methods, 2014.

31. Baptista, P.M., Siddiqui, M.M., Lozier, G., Rodriguez, S.R., Atala, A., and Soker, S. The use of whole organ decellularization for the generation of a vascularized liver organoid. Hepatology 53, 604, 2011.

32. Baptista, P.M., Orlando, G., Mirmalek-Sani, S.H., Siddiqui, M., Atala, A., and Soker, S. Whole organ decellularization - a tool for bioscaffold fabrication and organ bioengineering. Conf Proc IEEE Eng Med Biol Soc 2009, 6526, 2009.

33. Cartmell, J.S., and Dunn, M.G. Effect of chemical treatments on tendon cellularity and mechanical properties. J Biomed Mater Res 49, 134, 2000.

34. Deeken, C.R., White, A.K., Bachman, S.L., Ramshaw, B.J., Cleveland, D.S., Loy, T.S., and Grant, S.A. Method of preparing a decellularized porcine tendon using tributyl phosphate. J Biomed Mater Res B Appl Biomater 96, 199, 2011.

35. Gattazzo, F., Urciuolo, A., and Bonaldo, P. Extracellular matrix: A dynamic microenvironment for stem cell niche. Biochim Biophys Acta, 2014.

36. Jacot, J.G., McCulloch, A.D., and Omens, J.H. Substrate stiffness affects the functional maturation of neonatal rat ventricular myocytes. Biophys J 95, 3479, 2008.

37. Yeung, T., Georges, P.C., Flanagan, L.A., Marg, B., Ortiz, M., Funaki, M., Zahir, N., Ming, W., Weaver, V., and Janmey, P.A. Effects of substrate stiffness on cell morphology, cytoskeletal structure, and adhesion. Cell Motil Cytoskeleton 60, 24, 2005.

38. Raub, C.B., Mahon, S., Narula, N., Tromberg, B.J., Brenner, M., and George, S.C. Linking optics and mechanics in an in vivo model of airway fibrosis and epithelial injury. J Biomed Opt 15, 015004, 2010.

39. Raub, C.B., Putnam, A.J., Tromberg, B.J., and George, S.C. Predicting bulk mechanical properties of cellularized collagen gels using multiphoton microscopy. Acta Biomater 6, 4657, 2010.

40. Badylak, S.F., and Gilbert, T.W. Immune response to biologic scaffold materials. Semin Immunol 20, 109, 2008.

41. Weidemann, F., Herrmann, S., Stork, S., Niemann, M., Frantz, S., Lange, V., Beer, M., Gattenlohner, S., Voelker, W., Ertl, G., and Strotmann, J.M. Impact of myocardial fibrosis in patients with symptomatic severe aortic stenosis. Circulation 120, 577, 2009.

42. van Rooij, E., and Olson, E.N. MicroRNA therapeutics for cardiovascular disease: opportunities and obstacles. Nat Rev Drug Discov 11, 860, 2012.

43. Bhatia, S.N., Balis, U.J., Yarmush, M.L., and Toner, M. Microfabrication of hepatocyte/fibroblast co-cultures: role of homotypic cell interactions. Biotechnol Prog 14, 378, 1998.

44. Dixon, I.M., and Davies, J.J. Fibroblasts are coupled to myocytes in heart muscle by nanotubes: a bigger and better syncytium? Cardiovasc Res 92, 5, 2011.

45. Rinn, J.L., Bondre, C., Gladstone, H.B., Brown, P.O., and Chang, H.Y. Anatomic demarcation by positional variation in fibroblast gene expression programs. PLoS Genet 2, e119, 2006.

46. French, K.M., Boopathy, A.V., DeQuach, J.A., Chingozha, L., Lu, H., Christman, K.L., and Davis, M.E. A naturally derived cardiac extracellular matrix enhances cardiac progenitor cell behavior in vitro. Acta Biomater 8, 4357, 2012.

47. DeQuach, J.A., Mezzano, V., Miglani, A., Lange, S., Keller, G.M., Sheikh, F., and Christman, K.L. Simple and high yielding method for preparing tissue specific extracellular matrix coatings for cell culture. PLoS One 5, e13039, 2010.

48. Wainwright, J.M., Czajka, C.A., Patel, U.B., Freytes, D.O., Tobita, K., Gilbert, T.W., and Badylak, S.F. Preparation of cardiac extracellular matrix from an intact porcine heart. Tissue Eng Part C Methods 16, 525, 2010.

49. Eitan, Y., Sarig, U., Dahan, N., and Machluf, M. Acellular cardiac extracellular matrix as a scaffold for tissue engineering: in vitro cell support, remodeling, and biocompatibility. Tissue Eng Part C Methods 16, 671, 2010.

50. Payam Akhyari, H.A., Patricia Gwanmesia, Mareike Barth, Stefanie Hoffmann, Jorn Huelsmann, Karlheinz Preuss, Artur Lichtenberg. The Quest for an Optimized Protocol for Whole-Heart Decellularization: A Comparison of Three Popular and a Novel Decellularization Technique and Their Diverse Effects on Crucial Extracellular Matrix Qualities. Tissue Engineering: Part C 17, 11, 2011.

51. Jacot, J.G., Kita-Matsuo, H., Wei, K.A., Chen, H.S., Omens, J.H., Mercola, M., and McCulloch, A.D. Cardiac myocyte force development during differentiation and maturation. Ann N Y Acad Sci 1188, 121.

52. Engler, A.J., Carag-Krieger, C., Johnson, C.P., Raab, M., Tang, H.Y., Speicher, D.W., Sanger, J.W., Sanger, J.M., and Discher, D.E. Embryonic cardiomyocytes beat best on a matrix with heart-like elasticity: scar-like rigidity inhibits beating. J Cell Sci 121, 3794, 2008.

53. Shapira-Schweitzer, K., and Seliktar, D. Matrix stiffness affects spontaneous contraction of cardiomyocytes cultured within a PEGylated fibrinogen biomaterial. Acta Biomater 3, 33, 2007.

54. Hiltner, A., Cassidy, J.J., and Baer, E. Mechanical Properties of Biological Polymers. Annual Review of Materials Science 15, 455, 1985.

55. Maria Comninou, I.V.Y. Dependence of Stress-Strain Nonlinearity of Connective Tissue on the Geometry of Collagen Fibers. J. Biomechanics 9, 6, 1976.

56. Raub, C.B., Unruh, J., Suresh, V., Krasieva, T., Lindmo, T., Gratton, E., Tromberg, B.J., and George, S.C. Image correlation spectroscopy of multiphoton images correlates with collagen mechanical properties. Biophys J 94, 2361, 2008.

57. Christopher B. Raub, V.S., Tatiana Krasieva, Julia Lyubovitsky, Justin D. Mih, Andrew J. Putnam, Bruce J. Tromberg, Steven C. George. Noninvasive Assessment of Collagen Gel Microstructure and Mechanics Using Multiphoton Microscopy. Biophysical Journal 92, 10, 2007.

58. Badylak, S.F., Taylor, D., and Uygun, K. Whole-organ tissue engineering: decellularization and recellularization of three-dimensional matrix scaffolds. Annu Rev Biomed Eng 13, 27.

59. Zoumi, A., Yeh, A., and Tromberg, B.J. Imaging cells and extracellular matrix in vivo by using second-harmonic generation and two-photon excited fluorescence. Proc Natl Acad Sci U S A 99, 11014, 2002.

60. Richards-Kortum, R., and Sevick-Muraca, E. Quantitative optical spectroscopy for tissue diagnosis. Annu Rev Phys Chem 47, 555, 1996.

61. Robertson, C., and George, S.C. Theory and practical recommendations for autocorrelation-based image correlation spectroscopy. Journal of Biomedical Optics 17, 080801.

62. Mir, S.M., Baggett, B., and Utzinger, U. The efficacy of image correlation spectroscopy for characterization of the extracellular matrix. Biomed Opt Express 3, 215.

63. Akaike, H., Amari, S., Kitagawa, G., Kabashima, S., and Simodaira, H. Akaike Information Criterion. Math. Sci.(Tokyo) 14, 5, 1976.

64. Berry, M.F., Engler, A.J., Woo, Y.J., Pirolli, T.J., Bish, L.T., Jayasankar, V., Morine, K.J., Gardner, T.J., Discher, D.E., and Sweeney, H.L. Mesenchymal stem cell injection after myocardial infarction improves myocardial compliance. Am J Physiol Heart Circ Physiol 290, H2196, 2006.

65. Liu, F., Mih, J.D., Shea, B.S., Kho, A.T., Sharif, A.S., Tager, A.M., and Tschumperlin, D.J. Feedback amplification of fibrosis through matrix stiffening and COX-2 suppression. J Cell Biol 190, 693.

66. Puck, T.T., Cieciura, S.J., and Fisher, H.W. Clonal growth in vitro of human cells with fibroblastic morphology; comparison of growth and genetic characteristics of single epithelioid and fibroblast-like cells from a variety of human organs. J Exp Med 106, 145, 1957.

67. Bishop, J.E., and Lindahl, G. Regulation of cardiovascular collagen synthesis by mechanical load. Cardiovasc Res 42, 27, 1999.

68. Scaffidi, A.K., Moodley, Y.P., Weichselbaum, M., Thompson, P.J., and Knight, D.A. Regulation of human lung fibroblast phenotype and function by vitronectin and vitronectin integrins. J Cell Sci 114, 3507, 2001.

69. Reynolds, L.E., Conti, F.J., Lucas, M., Grose, R., Robinson, S., Stone, M., Saunders, G., Dickson, C., Hynes, R.O., Lacy-Hulbert, A., and Hodivala-Dilke, K. Accelerated re-epithelialization in beta3-integrin-deficient- mice is associated with enhanced TGF-beta1 signaling. Nat Med 11, 167, 2005.

70. Wang, H.J., Pieper, J., Schotel, R., van Blitterswijk, C.A., and Lamme, E.N. Stimulation of skin repair is dependent on fibroblast source and presence of extracellular matrix. Tissue Eng 10, 1054, 2004.

71. Crapo, P.M., Gilbert, T.W., and Badylak, S.F. An overview of tissue and whole organ decellularization processes. Biomaterials 32, 3233, 2011.

72. Freytes, D.O., Martin, J., Velankar, S.S., Lee, A.S., and Badylak, S.F. Preparation and rheological characterization of a gel form of the porcine urinary bladder matrix. Biomaterials 29, 1630, 2008.

73. Raghu, G., Masta, S., Meyers, D., and Narayanan, A.S. Collagen synthesis by normal and fibrotic human lung fibroblasts and the effect of transforming growth factor-beta. Am Rev Respir Dis 140, 95, 1989.

74. Elias, J.A., Freundlich, B., Adams, S., and Rosenbloom, J. Regulation of human lung fibroblast collagen production by recombinant interleukin-1, tumor necrosis factor, and interferon-gamma. Ann N Y Acad Sci 580, 233, 1990.

75. Lijnen, P.J., Petrov, V.V., and Fagard, R.H. Collagen production in cardiac fibroblasts during inhibition of angiotensin-converting enzyme and aminopeptidases. J Hypertens 22, 209, 2004.

76. Siwik, D.A., Chang, D.L., and Colucci, W.S. Interleukin-1beta and tumor necrosis factor-alpha decrease collagen synthesis and increase matrix metalloproteinase activity in cardiac fibroblasts in vitro. Circ Res 86, 1259, 2000.

77. Zhang, H.Y., Gharaee-Kermani, M., Zhang, K., Karmiol, S., and Phan, S.H. Lung fibroblast alpha-smooth muscle actin expression and contractile phenotype in bleomycin-induced pulmonary fibrosis. Am J Pathol 148, 527, 1996.

78. Mariani, T.J., Arikan, M.C., and Pierce, R.A. Fibroblast tropoelastin and alpha-smooth-muscle actin expression are repressed by particulate-activated macrophage-derived tumor necrosis factor-alpha in experimental silicosis. Am J Respir Cell Mol Biol 21, 185, 1999.

79. Lijnen, P., and Petrov, V. Transforming growth factor-beta 1-induced collagen production in cultures of cardiac fibroblasts is the result of the appearance of myofibroblasts. Methods Find Exp Clin Pharmacol 24, 333, 2002.

80. Pelham, R.J., Jr., and Wang, Y. Cell locomotion and focal adhesions are regulated by substrate flexibility. Proc Natl Acad Sci U S A 94, 13661, 1997.

81. Solon, J., Levental, I., Sengupta, K., Georges, P.C., and Janmey, P.A. Fibroblast adaptation and stiffness matching to soft elastic substrates. Biophys J 93, 4453, 2007.

82. Georges, P.C., and Janmey, P.A. Cell type-specific response to growth on soft materials. J Appl Physiol 98, 1547, 2005.

83. van den Borne, S.W., Diez, J., Blankesteijn, W.M., Verjans, J., Hofstra, L., and Narula, J. Myocardial remodeling after infarction: the role of myofibroblasts. Nat Rev Cardiol 7, 30, 2010.

84. Desmouliere, A., Chaponnier, C., and Gabbiani, G. Tissue repair, contraction, and the myofibroblast. Wound Repair Regen 13, 7, 2005.

85. Gabbiani, G. The myofibroblast in wound healing and fibrocontractive diseases. J Pathol 200, 500, 2003.

86. Kim, B.S., Choi, J.S., Kim, J.D., Choi, Y.C., and Cho, Y.W. Recellularization of decellularized human adipose-tissue-derived extracellular matrix sheets with other human cell types. Cell Tissue Res 348, 559, 2012.

87. Margadant, C., and Sonnenberg, A. Integrin-TGF-beta crosstalk in fibrosis, cancer and wound healing. EMBO Rep 11, 97.

88. Burgess, H.A., Daugherty, L.E., Thatcher, T.H., Lakatos, H.F., Ray, D.M., Redonnet, M., Phipps, R.P., and Sime, P.J. PPARgamma agonists inhibit TGF-beta induced pulmonary myofibroblast differentiation and collagen production: implications for therapy of lung fibrosis. Am J Physiol Lung Cell Mol Physiol 288, L1146, 2005.

89. Phan, S.H. The myofibroblast in pulmonary fibrosis. Chest 122, 286S, 2002.

APPENDIX A

TGF-β	50ng/mL TGF-β
TNF-α	100ng/mL TNF-α
coll coat	1mg/mL type 1 collagen in 0.1M acetic acid for 1 hour at 37 C
FN coat	Coated at 25µg/mL fibronectin for 1 hour at 37 C
LECM1 coat	Porcine lung tissue decellularized by 1% sodium docecyl sulfate for 4-5 days, rinsed with Triton X-100 for 30 min, and deionized water overnight. Then milled into a fine powder, digested in pepsin and coated at 1mg/mL in 0.1M acetic acid for 1 hour at 37 C
CECM1 coat	Porcine ventricular tissue decellularized by 1% sodium docecyl sulfate for 4-5 days, rinsed with Triton X-100 for 30 min, and deionized water overnight. Then milled into a fine powder, digested in pepsin and coated at 1mg/mL in 0.1M acetic acid for 1 hour at 37 C
CECM2 coat	Porcine ventricular tissue decellularized by 0.02% Trypsin/0.05% EDTA/0.05% NaN_3 for 1 day and 3% Triton X-100/0.05% EDTA/0.05% NaN_3 for 6 days. Desiccated, reduced to powder, treated with pepsin for 4 days, and coated at 1mg/mL in 0.1M acetic acid for 1 hour at 37 C
CECM3 coat	Porcine ventricular tissue decellularized by 0.02% Trypsin/0.05% EDTA/0.05% NaN_3 for 3 days and 3% Triton X-100/0.05% EDTA/0.05% NaN_3 for 4 days. Desiccated, reduced to powder, treated with pepsin for 4 days, and coated at 1mg/mL in 0.1M acetic acid for 1 hour at 37 C
coll gel	10mg/mL type 1 collagen at pH 8.5 (2mL gel) for 1 hour at 37 C
CECM1 intact	Porcine ventricular tissue decellularized by 0.02% Trypsin/0.05% EDTA/0.05% NaN_3 for 1 day and 3% Triton X-100/0.05% EDTA/0.05% NaN_3 for 6 days
CECM2 intact	Porcine ventricular tissue decellularized by 0.02% Trypsin/0.05% EDTA/0.05% NaN_3 for 3 days and 3% Triton X-100/0.05% EDTA/0.05% NaN_3 for 4 days

Table A.1: Conditions

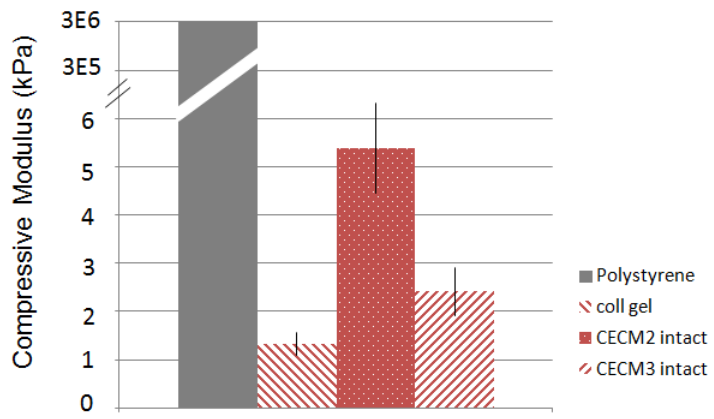

FIG A.1: Compressive modulus of acellular gels and C-ECM samples, measured via indentation testing.

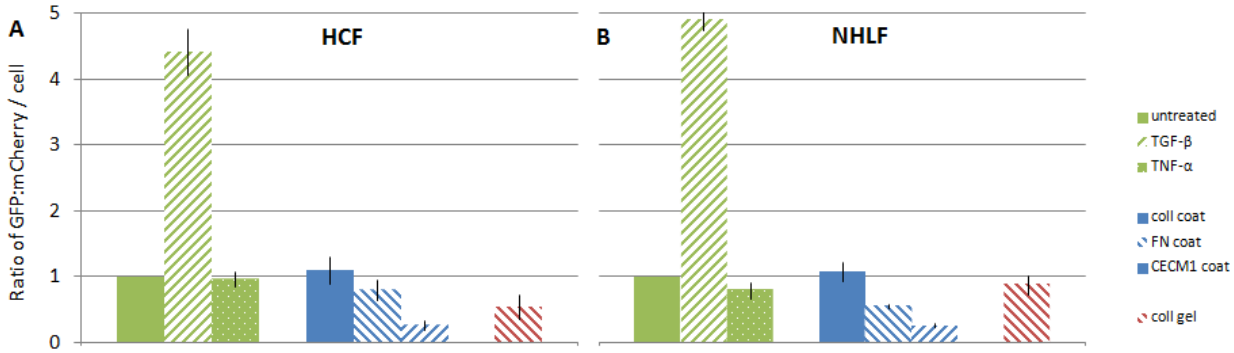

FIG A.2: GFP Human collagen 1 promoter reporter and constitutively expressed mCherry non-viral plasmids co-transfected into NHLFs and HCFs. The ratio of GFP to mCherry fluorescence was measured on a per cell basis using ImageJ and normalized to untreated fibroblasts.